SÃO PAULO UNIVERSITY
SÃO CARLOS SCHOOL OF ENGINEERING

Jonathan Campo Jaimes

Ankle torque estimation for Lower-Limb Robotic Rehabilitation

São Carlos

2018

Jonathan Campo Jaimes

Estimativa de torque no tornozelo para reabilitação robótica de membros inferiores

Dissertação apresentada à Escola de Engenharia de São Carlos da Universidade de São Paulo, para obtenção do título de Mestre em Ciências - Programa de Pós-Graduação em Engenharia Mecânica.

Área de concentração: Dinâmica e Mecatrônica

Orientador: Adriano Almeida Gonçalves Siqueira

São Carlos

2018

Jonathan Campo Jaimes

Ankle torque estimation for Lower-Limb Robotic Rehabilitation

A dissertation submitted to the Sao carlos School of Engineering at Sao Paulo University, in fulfillment of the requirements for the degree of Master of Science - Mechanical Engineering Postgraduate Program

Concentration area: Dynamics and Mechatronics

Supervisor: Adriano Almeida Gonçalves Siqueira

THIS EXEMPLARY IS THE CORRECTED VERSION. THE ORIGINAL VERSION IS AVAILABLE AT THE EESC-USP DEPARTMENT OF MECHANICAL ENGINEERING.

São Carlos

2018

FOLHA DE JULGAMENTO

Candidato: Engenheiro **JONATHAN CAMPO JAIMES.**

Título da dissertação: "Estimativa de torque no tornozelo para reabilitação robótica de membros inferiores".

Data da defesa: 15/06/2018.

Comissão Julgadora:	**Resultado:**
Prof. Associado **Adriano Almeida Gonçalves Siqueira (Orientador)** (Escola de Engenharia de São Carlos/EESC)	Aprovado
Prof. Dr. **Valdir Grassi Junior** (Escola de Engenharia de São Carlos/EESC)	Aprovado
Prof. Dr. **Álvaro David Orjuela Caño** (Universidade Antonio Nariño/UAN-Colômbia)	Aprovado

Coordenador do Programa de Pós-Graduação em Engenharia Mecânica:
Prof. Associado **Gherhardt Ribatski**

Presidente da Comissão de Pós-Graduação:
Prof. Associado **Luís Fernando Costa Alberto**

RESUMO

CAMPO, J. **Estimativa de torque no tornozelo para reabilitação robótica de membros inferiores**. 2018. 57p. Dissertação (Mestrado) - Escola de Engenharia de São Carlos, Universidade de São Paulo, São Carlos, 2018.

Em terapias de reabilitação robótica, o conhecimento dos torques da articulação humana é importante para a segurança do paciente, para fornecer dados confiáveis na avaliação clínica e aumentar o desempenho de controle do dispositivo, no entanto, sua medição pode ser complexa ou costoso de implementar. A maioria das técnicas de estimativa de torque tem sido desenvolvidas para dispositivos de reabilitação robótica de membros superiores, além disso, eles normalmente requerem modelos antropométricos e musculoesqueléticos detalhados. Nesta dissertação é apresentada a estimativa do torque do tornozelo no robô Anklebot, a estimação utiliza um modelo dinâmico tornozelo + Anklebot o qual considera a medição da posição e velocidade angular do tornozelo, os parametros de impedancia mecânica do tornozelo são obtidos por meio de um modelo simples de segunda ordem e são identificados os torques gravitacionais e de atrito. Três abordagens para a estimativa de torque de tornozelo foram propostas para serem implementadas, o momento generalizado, o filtro de Kalman e, finalmente, uma abordagem que combina tanto o momento generalizado e o filtro de Kalman. A validação de tais abordagens foi desenvolvida primeiro em um *mock-up* físico configurado para reproduzir o movimento articular do tornozelo humano, avaliando seus desempenhos. A segunda abordagem proposta foi selecionada para ser implementada em um usuário voluntário. Um conjunto de experimentos foi realizado considerando a atividade física que o sujeito pode realizar ao interagir com o Anklebot, a estimativa desenvolvida de torque de tornozelo demostrou ser bem sucedida para o torque passivo e na maioria dos cenários propostos onde o torque ativo é realizado.

Palavras-chave: Torque no tornozelo, Algoritmos de estimação, Reabilitação Robótica, Estratégias de Controle,Interação humano-robô.

ABSTRACT

CAMPO, J. **Ankle torque estimation for Lower-Limb Robotic Rehabilitation**. 2018. 59p. Dissertation (Master) - São Carlos School of Engineering, São Paulo University, São Carlos, 2018.

In robotic rehabilitation therapies, knowledge of human joint torques is important for patient safety, to provide a reliable data for clinical assessment and to increase control performance of the device, nevertheless, its measurement can be complex or have a high-cost implementation. The most of techniques for torque estimation have been developed for upper limb robotic rehabilitation devices, in addition, they typically require detailed anthropometric and musculoskeletal models. In this dissertation is presented the ankle torque estimation for the Anklebot robot, the estimation uses an ankle/Anklebot dynamic model that consider the ankle joint angular displacement and velocity measurement, its mechanical impedance parameters are obtained through a second-order modeled mechanical impedance of the ankle and an identification of frictional and gravitational torques. Three approaches for the ankle torque estimation were proposed to be implemented in the Anklebot robot, the Generalized Momentum, the Kalman filter and finally a combination of both the above mentioned approaches. The validation of such approaches was developed first on a physical mockup configured to reproduce the human ankle joint movement, by assessing its performances, the Kalman filter approach was selected to be implemented on a voluntary subject. A set of experiments were performed considering the physical activity that the subject may realize when interacting with the Anklebot, the developed ankle torque estimation proved to be successful for passive torque and in most of the proposed scenarios where active torque is performed.

Keywords: Ankle Torque, Estimation Algoritms, Robotic Rehabilitation, Control Strategies, Human-Robot Interaction.

LIST OF FIGURES

LIST OF TABLES

CONTENTS

1 INTRODUCTION

1.1 Motivation

Over time, advances in the development of rehabilitation robots have helped therapists in their efforts to facilitate the patients functional recovery, since these robots must have direct physical interaction with patients, safety is a critical concern. Most rehabilitation robots initially only provided training in passive mode, that is, the robot guides the patient's extremities along a desired trajectory (PRANGE et al., 2006). In recent years, many researchers have insisted that robotic assistance should be adaptable according to the patient's contribution to more effective and optimal training (RIENER et al., 2005; CAI et al., 2006).

Therapists support the Assist-As-Needed rehabilitation paradigm, which states that robotic interventions must be tailored to the requirements of each subject and their use minimized only to situations for which the subject truly requires them (PRIETO GUILLERMO, 2014). According to Riener et al. (2005), in robotic therapy the muscular effort quantification is important to make adaptable the robot behavior and to inform about the patient progress in a training. The joint torque, as well as other biomechanical parameters, are related to the muscular effort expended in a physical activity (ANDREWS, 1983), Thus, knowing the joint torque is essential to quantify the patient's contribution in a physical therapy (LUNENBURGER; COLOMBO; RIENER, 2007).

1.2 State of art

Strength which is directly associated with torque, has been measured using manual muscle testing (MMT) or isokinetic torque measurement systems. MMT is easy to perform as it does not require any specific equipment but it has a low reliability (ESCOLAR et al.,) and low sensitivity (BOHANNON, 2005). By using isokinetic/isometric measurement systems it is possible to assess strong functions more reliably, but they have the disadvantage of being rather expensive. To summarize, depending on the robotic system, the above mentioned measurements can be technically difficult to realize or could be very expensive to implement. Currently in the research field of robotic rehabilitation, there exists the interest in finding alternative approaches to estimate the patient torque based on others measurements that simplify this task.

Due to the complex interaction between the mechanical characteristics of a muscle and its electrical activity, electromyography (EMG) has been a well-studied methodology to estimate the patient's torque during rehabilitation therapy (PEñA; JAUREGUI; SIQUEIRA,

2015; LLOYD; BESIER, 2003; KOMADA et al., 2009; ERDEMIR et al., 2007). Although the measurement of EMG signals has advantages in terms of detecting the user's intentions with precise time, it has practical limitations, for example, electrode fixation is time-consuming, also complex signal processing and calibration measurement are required.

In Hussain, Xie e Jamwal (2013), the interaction torques between a robotic orthosis and its user were identified through load cells, where a model of inverse dynamics of the human-robot system was used to isolate the active torque component from the passive effects and kinetic modeling. In Kim et al. (2014), Lenzi et al. (2011) and Khan et al. (2015) similar procedures are developed by pressure sensors to measure interaction torques.

Some methods for force estimation and sensorless force control have been developed for robotic manipulators. The Disturbance Observers (DOB), originally presented in Ohnishi (1987), has been used to estimate external forces and torques of a manipulator by using only encoders (MURAKAMI; YU; OHNISHI, 1993), (EOM et al., 1998) and more recently (MAQUIN et al., 2015). The DOB idea is to consider a dynamic system with external disturbances and use a state observer to estimate and compensate for disturbances within a control system. The DOB has the advantages of requiring only joint angle measurement and actuator signals (current, voltage and torque in the motor), furthermore eliminates the need for acceleration measures and does not require inversion of the inertia matrix of the dynamic system robotic. The DOB has already been used in estimating torque in robotic systems of rehabilitation for upper limbs (ABHISHEK; K., 2010; UGURLU et al., 2012; UGURLU et al., 2015) showing acceptable results, however, the effectiveness of the estimation depends on accurate mathematical modeling of the human-robot system as well a good compensation of the frictional forces and other non-linear effects.

An alternative approach was proposed in Luca e Mattone (2003a) to estimate disturbance torques in robotic manipulators. It generates diagnostic signals named as *residues* in correspondence with potential faults (disturbances) that can affect the system. This approach takes advantage of the mechanical property of the generalized momentum of the robot, which has the advantage of decoupling the torque from the disturbance with respect to the dynamic system. Therefore, this method works independently of the nominal torque generation scheme. In addition, it does not need to reverse the inertia matrix which makes it possible to incorporate linear control techniques while fully utilizing system nonlinearities.

Another approach has proven to be very efficient in robotic manipulators is the Kalman filter which was used in Park e Chung (2013) to estimate external torques in the joints in a robotic system. The Kalman filter is a recursive algorithm that estimates the complete

state vector of a dynamic system disturbed by Gaussian white noise from partial state measurements. In (JUNG; LEE; HUH, 2006), an extended structure of the Kalman filter is combined with the Lyapunov's law of adaptation to estimate the contact force of a nonlinear model for the manipulator robot. In Wahrburg et al. (2015) the external torque of a 7-DoF manipulator is estimated by using an approach that combines the Kalman filter based and the Generalized momentum, the estimated torque was modeled as a linear system.

Some estimation strategies like the non-linear disturbance observer (STEFAN; NATHAN; HENK, 1993) and extended Kalman Filter (RADKE; GAO, 2006; KIM; CHO; CHOI, 2016) have been implemented to estimate external torques in robotic manipulators and even in robotic devices for upper limb rehabilitation. Nevertheless, there exists a lack of applications of this estimation strategies in the lower limb robotic rehabilitation field.

This thesis is focused in the development of a nominal estimation approach on a robotic device for lower limbs rehabilitation, The developed torque estimation is a good starting point in the search for future robust estimation methods.

1.3 Objectives

The main goal of this thesis is to develop an ankle torque estimation to be used in robotic rehabilitation therapies. The estimation will be implemented on the Anklebot which is a robot device for ankle rehabilitation. This robot will be delimited to operate in dorsi-plantar flexion.

The following estimation approaches are discussed in the thesis:

1. Generalized momentum;
2. Kalman filter;
3. Combined Kalman filter and Generalized momentum.

Before estimating the ankle torque of a subject wearing the Anklebot, the approaches needs to be validated, hence, they are tested first on an physical mock-up assembled to replicate the human ankle movement in the sagittal plane. In order to perform the torque estimation, a detailed ankle/Anklebot dynamic model is required. This model is developed considering the mechanical impedance parameters of the whole Ankle and Anklebot system, including the gravitational and frictional torques.

1.4 Thesis Outline

Chapter 2 provides the background for the proposed approaches for ankle torque estimation. Chapter 3 describes a system modeling of the Anklebot/ankle dynamics. Chapter 4 shows

the validation and performance assessment for the selection of the appropriate approach. Finally in chapter 5, the implementation of the Kalman filter approach to estimate the ankle torque of a voluntary subject is presented.

2 TORQUE ESTIMATION APPROACHES

This chapter presents the methods proposed for ankle torque estimation. They are formulated under the concept of observing the disturbance input of a feedback control system. In this work the ankle torque is considering as the disturbance to be estimated.

2.1 Generalized momentum observer approach

The generalized momenta observer approach (DAMME et al., 2011) assumes the presence of a disturbance torque, τ_d, in the robotic device joints as result of the interaction of the robot with its environment (LUCA; MATTONE, 2003b; LUCA; MATTONE, 2005; LUCA et al., 2006).

Conventionally, the inverse model of robotic systems are given in the form:

$$M(\theta)\ddot{\theta} + C(\dot{\theta}, \theta)\dot{\theta} + G(\theta) + \tau_{fric}(\dot{\theta}) = \tau_r - \tau_d \tag{2.1}$$

where $\theta \in \mathbb{R}^n$ denotes the vector of joint angles, n is the degree of freedom (DoF) of the robot system; $M \in \mathbb{R}^{n \times n}$ is the positive definitive inertia matrix; the term $C(\dot{\theta}, \theta)\dot{\theta} \in \mathbb{R}^n$ joins the Coriolis and conservative torques, and $G(\theta) \in \mathbb{R}^n$ represent the gravitational torques. The torques acting at the joints are the applied by the actuator $\tau_r \in \mathbb{R}^n$, the friction torque τ_{fric} and the disturbance torque $\tau_d \in \mathbb{R}^n$ due to interaction a physical environment.

According to (SICILIANO et al., 2009), the matrix $C(q, \dot{q})$ can be expressed by:

$$\dot{M}(\theta) = C(\theta, \dot{\theta}) + C^T(\theta, \dot{\theta}). \tag{2.2}$$

The proposed disturbance observer is based on the generalized momenta, defined as:

$$p = M(\theta)\dot{\theta}. \tag{2.3}$$

Its time derivative is given by:

$$\dot{p} = M(\theta)\ddot{\theta} + \dot{M}(\theta)\dot{\theta}. \tag{2.4}$$

Substituting (2.1) and (2.2) into (2.4), one obtains:

$$\dot{p} = \tau_r + C^T(\theta, \dot{\theta})\dot{\theta} - G(\theta) - \tau_{fric}(\dot{\theta}) - \tau_d. \tag{2.5}$$

This equation demonstrates the advantage of using the generalized momenta, since the evolution of p is decoupled from the torque disturbance, and the i-th component of $\dot{p}$ only depends on the i-th component of τ_d.

At this point, it is assumed that the objective is to develop an observer to p instead of τ_d. Thus, ignoring the term τ_d for not being a measurement information, and inserting an entry containing the prediction error $e = p - \hat{p}$, where $\hat{p}$ is a predictor of p, the dynamics of the observer is given by:

$$\dot{\hat{p}} = \tau_r + C^T(\theta, \dot{\theta})\dot{\theta} - G(\theta) - \tau_{fric}(\dot{\theta}) + K_I e, \tag{2.6}$$

where K_I is a positive-definite diagonal gain matrix.

Provided there are no uncertainties in system modeling, it is verified that $K_I e$ corresponds to τ_d. Writing $r = K_I e$, by means of (2.5) and (2.6), one obtains:

$$\dot{r} = K_I(\dot{p} - \dot{\hat{p}}) = K_I\tau_d - K_I r. \tag{2.7}$$

Finally, an estimation for the disturbance torque can be computed as:

$$\hat{\tau}_d = \frac{\dot{r}}{K_I} + r. \tag{2.8}$$

The estimated disturbance torque can be expressed in the Laplace domain:

$$r(s) = \frac{K_I}{s + K_I}\tau_d(s), \tag{2.9}$$

That is, r is the result of applying the disturbance torque through a first-order low pass filter, namely, r is a smoothed version of $\hat{\tau}_d$.

2.2 Linearized Kalman filter approach

2.2.1 Augmented state-space system

From the system dynamic model (Equation 2.1) an expression defining the angular acceleration can be obtained:

$$\ddot{\theta} = M(\theta)^{-1}\left[\tau_r - \tau_d - C(\dot{\theta}, \theta)\dot{\theta} - G(\theta) - \tau_{fric}(\dot{\theta})\right]. \tag{2.10}$$

For notation simplicity, (2.10) is rewritten as:

$$\ddot{\theta} = M^{-1}\left[\tau_r - \tau_d - C\dot{\theta} - G - \tau_{fric}\right], \tag{2.11}$$

and represented as a continuous-time state-space equation:

$$\begin{bmatrix} \ddot{\theta} \\ \dot{\theta} \end{bmatrix} = \begin{bmatrix} -CM^{-1} & -GM^{-1} \\ 0 & 0 \end{bmatrix} \begin{bmatrix} \dot{\theta} \\ \theta \end{bmatrix} + \begin{bmatrix} M^{-1} \\ 0 \end{bmatrix} \tau_r - \begin{bmatrix} M^{-1} \\ 0 \end{bmatrix} \tau_d - \begin{bmatrix} M^{-1} \\ 0 \end{bmatrix} \tau_{fric}. \tag{2.12}$$

A common approach for disturbance rejection in control systems design, is to assume that the structure of the disturbance is known (RADKE; GAO, 2006; MUSKE; BADGWELL, 2002). If the disturbance has a sinusoidal behavior, then, the mathematical model generating such a signal is given by:

$$\tau_d = A_d \sin(\omega_0 t) \tag{2.13}$$

and its derivative and integral functions:

$$\dot{\tau_d} = A_d \omega_0 \cos(\omega_0 t), \tag{2.14}$$

$$\int \tau_d = -\frac{A_d}{\omega_0} \sin(\omega_0 t). \tag{2.15}$$

Therefore, the disturbance model can be rearranged in state space form:

$$\begin{bmatrix} \dot{\tau_d} \\ \tau_d \end{bmatrix} = \begin{bmatrix} 0 & -\omega_0^2 \\ 1 & 0 \end{bmatrix} \begin{bmatrix} \tau_d \\ \int \tau_d \end{bmatrix} \tag{2.16}$$

It is worth notice that the physical meaning of torque integral is the angular impulse ($kg\, m^2/s$ units). By augmenting the system (2.12) with the state-space model (2.16), the disturbance and its integral value can be regarded as state variables:

$$\begin{bmatrix} \ddot{\theta} \\ \dot{\theta} \\ \dot{\hat{\tau}}_d \\ \dot{\tau}_d \end{bmatrix} = \underbrace{\begin{bmatrix} -CM^{-1} & -GM^{-1} & -M^{-1} & 0 \\ 1 & 0 & 0 & 0 \\ 0 & 0 & 0 & -\omega_0^2 \\ 0 & 0 & 1 & 0 \end{bmatrix}}_{A_c} \underbrace{\begin{bmatrix} \dot{\theta} \\ \theta \\ \hat{\tau}_d \\ \int \hat{\tau}_d \end{bmatrix}}_{x} + \underbrace{\begin{bmatrix} M^{-1} \\ 0 \\ 0 \\ 0 \end{bmatrix}}_{B_c} \underbrace{(\tau_r - \tau_{fric})}_{u}, \tag{2.17}$$

where A_c and B_c are the continuous state transition and input matrices respectively, x the state vector and u the input system. Since θ and $\dot{\theta}$ are the measurable variables of the state vector, an output system equation is defined as:

$$y = \underbrace{\begin{bmatrix} 1 & 0 & 0 & 0 \\ 0 & 1 & 0 & 0 \end{bmatrix}}_{H} \underbrace{\begin{bmatrix} \dot{\theta} \\ \theta \\ \tau_d \\ \int \tau_d \end{bmatrix}}_{x}. \tag{2.18}$$

2.2.2 **Discrete Kalman filter algorithm**

Is important to note that the augmented model described by Equations (2.17) and (2.18) has nonlinear components, then it can be expressed as a function:

$$\dot{x} = f(x(t), u(t), t), \tag{2.19}$$

thus, a linearization of the process model about an equilibrium point $\bar{x}$ that satisfy $f(\bar{x}, \bar{u}) = 0$ where $\bar{u}$ is the corresponding equilibrium input, yield the constant matrices:

$$A = \left.\frac{\partial f}{\partial x}\right|_{x=\bar{x},u=\bar{u}} \qquad B = \left.\frac{\partial f}{\partial u}\right|_{x=\bar{x},u=\bar{u}}. \tag{2.20}$$

An important aspect for the discrete kalman filter implementation is that the transition matrix A of the linearized model is calculated at each time with the most recent state estimate, which is assumed to be the corrected estimated.

Now, the linearized augmented model can be discretized resulting in the time-varying, discrete-time linear system in the form:

$$x_k = A_k x_{k-1} + B_k u_k + w_{k-1}, \tag{2.21}$$

$$z_k = H x_k + v_k. \tag{2.22}$$

The discrete Kalman filter explained in this section is a summarized version of the presented in Welch e Bishop (2001). The Kalman filter addresses the general problem of trying to estimate the state $x \in \mathbb{R}^n$ of a discrete-time controlled process that is governed by the linear stochastic difference equation (2.21). with a measurement $z \in \mathbb{R}^m$ (Equation 2.22).

The random variables w_k and v_k represent the process and measurement noise respectively. They are assumed to be independent (of each other), white, and with normal probability distributions

$$p(w) \sim N(0, Q), \tag{2.23}$$

$$p(v) \sim N(0, R). \tag{2.24}$$

where Q and R are the process noise and measurement noise covariance matrices.

The Kalman filter estimates a process by using a form of feedback control: the filter estimates the process state at some time and then obtains feedback in the form of (noisy) measurements. As such, the equations for the Kalman filter fall into two groups: *time update* equations and *measurement update* equations. The time update equations are responsible for projecting forward (in time) the current state and error covariance estimates to obtain the *a priori* estimates for the next time step. The measurement update equations are responsible for the feedback i.e. for incorporating a new measurement into the *a priori* estimate to obtain an improved *a posteriori* estimate. Indeed the final estimation algorithm resembles that of a *predictor-corrector* algorithm for solving numerical problems as shown below in Figure (1).

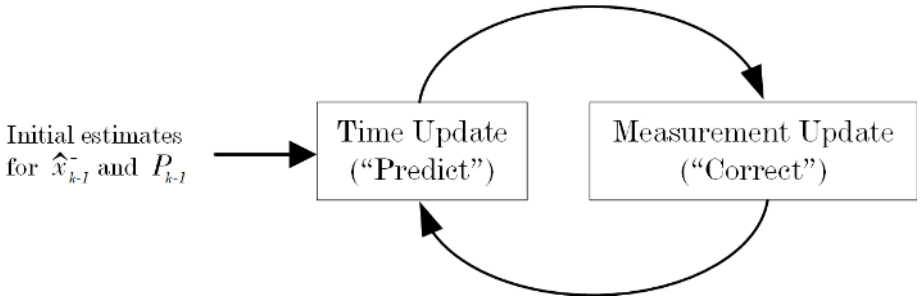

Figure 1: The discrete Kalman filter cycle.

The specific equations for the time update are:

$$\hat{x}_k^- = A\hat{x}_{k-1} + Bu_k \tag{2.25}$$

$$P_k^- = AP_{k-1}A^T + Q \tag{2.26}$$

Notice how the time update equations project the state and covariance estimates forward from time step $k-1$ to step k. A and B are from equation (2.21), while Q is from equation (2.23). Initial conditions for the filter are discussed in the earlier references.

The specific equations for measurement update are:

$$K_k = P_k^- H^T \ (HP_k^- H^T + R)^{-1} \tag{2.27}$$

$$\hat{x}_k = \hat{x}_k^- + K_k \ (z_k - H\hat{x}_k^-), \tag{2.28}$$

$$P_k = (I - K_k H)P_k^- \tag{2.29}$$

The first task during the measurement update is to compute the Kalman gain, K_k. The next step is to actually measure the process to obtain z_k, and then to generate an *a posteriori* state estimate by incorporating the measurement as in equation (2.28). The final step is to obtain an a posteriori error covariance estimate via equation (2.29).

After each time and measurement update pair, the process is repeated with the previous *a posteriori* estimates used to project or predict the new *a priori* estimates.

2.3 Combined Kalman filter and Generalized momentum approach

The third approach proposed to estimate the ankle torque, involves a combination of the generalized momentum described in section 2.1 and the Kalman filter in in section 2.2.2. This combined approach was originally proposed in Wahrburg et al. (2015) to estimate external forces of a 7-DoF manipulator. In addition to the advantage of just require the available motor signals (currents, angles, speeds), the authors remarks that this approach allows improving the force estimation quality compared to existing approaches by exploiting additional information regarding uncertainty in the joint friction estimates.

As described in Section (2.1), the robotic dynamic model (Equation 2.1) can be rewritten as:

$$\dot{p} = \tau_r + C^T\dot{\theta} - G - \tau_{fric} - \tau_d. \tag{2.30}$$

Focusing on estimating the external torque, thus, unlike Section (2.1) where the friction model is modeled, here $\hat{\tau}_{fric}$ is assumed to be available, where uncertainties in friction estimates (considered to have highest significance for the dynamic system) are modeled as random variables, i.e.

$$w_p = \hat{\tau}_{fric} - \tau_{fric} \sim N(0, Q_{c,p}) \tag{2.31}$$

Introducing the abbreviation $\bar{\tau} = \tau_r + C^T\dot{\theta} - G - \tau_{fric}$ the dynamics equation (2.30) is then expressed as:

$$\dot{p} = \bar{\tau} - \tau_d + w_p, \tag{2.32}$$

where w_p is a noise term. For an accurate model, the term w_p will be dominated by uncertainties in the friction model. Such model is modeled as $w_p \sim N(0, Q_{c,p})$.

The key idea is to combine the description of the manipulator dynamics based on the generalized momentum with well known disturbance observer approaches. To this end, the external torque is modeled as:

$$\dot{\tau_d} = A_d\tau_d + w_d, \tag{2.33}$$

where A_d determines the dynamics assumed of the external torque, its subscript refers that the torque is considered as a disturbance. If A_d is chosen as 0, the external torque is considered to be constant with its derivative being subject to noise (w_d in Equation 2.33).

Defining the state vector $x = [p^T \;\; \tau_d^T]^T$ and combining the noise equations as $w = [w_p^T \;\; w_d^T]^T$, equations (2.30) and (2.33) can be rearranged to form the augmented system:

$$\underbrace{\begin{bmatrix} \dot{p} \\ \dot{\tau_d} \end{bmatrix}}_{\dot{x}} = \underbrace{\begin{bmatrix} 0 & -1 \\ 0 & A_f \end{bmatrix}}_{A_c} \underbrace{\begin{bmatrix} p \\ \tau_d \end{bmatrix}}_{x} + \underbrace{\begin{bmatrix} 1 \\ 0 \end{bmatrix}}_{B_c} + \underbrace{\bar{\tau}}_{u} + w. \tag{2.34}$$

taking into account that the momentum can be measured as $p = M\dot{\theta}$, and assuming measurement noise $v \sim N(0, R_c)$, the output equation of the augmented system can be written as:

$$p = \underbrace{[1 \quad 0]}_{H} \underbrace{\begin{bmatrix} p \\ \tau_d \end{bmatrix}}_{x} + v. \tag{2.35}$$

Once an augmented system is defined, the discrete Kalman algorithm of Section (2.2.2) can be implemented to estimate both the measured momentum and the unknown external torque (considered as disturbance).

3 SYSTEM MODELING

3.1 The Anklebot

The Anklebot (**??**) is a backdriveable robot with low intrinsic mechanical impedance, designed to help people who have suffered from brain damage in restoring the range of motion, passive stiffness and strength of the ankle. During robotic therapy, the Anklebot is attached to the patient's affected leg with a knee pad and a generic orthotic shoe.

Figure 2: The Anklebot. Font: **??**).

Two linear actuators mounted in parallel to the leg move the ankle joint in the three degrees of freedom, where the dorsiflexion-plantarflexion (DP) and inversion-eversion (IE) movements are actuated. The ankle robot allows 25° of dorsiflexion, 45° of plantarflexion, 25° of inversion, 20° of eversion, and 15° of internal or external rotation. The Anklebot can apply torque of up to 23 N/m for DP and 15 N/m for IE. The Anklebot is provided by two types of encoders; a a set of Gurley R119 rotational encoders mounted coaxial with the motors with a resolution of 8,78 x 10 $^{-3}$ ° and a set of Renishaw incremental linear encoders mounted on the traction drive with a resolution of 5 x 10^{-6} m.

The schematic of the Anklebot in sagittal plane is presented in Figure 3. To determine the angular position θ_{DP} and the actuator torque, τ_{DP}, it uses a linearized mathematical and geometric model of the leg-ankle-foot system based on average anthropometric values and measurements of the linear position sensors, X_L and X_R, as well as the linear force sensors, F_L e R_R:

$$\tau_{DP} = (F_R + F_L)x_{length} \tag{3.1}$$

$$\theta_{DP} = \theta_{DP,offset} + tan^{-1}\left(\frac{X_R + X_L}{x_{length}}\right) \tag{3.2}$$

where the sub-indexes R and L refers to the left and right individual actuators, respectively, x_{length} is the distance between the line of action of actuator force and the point of

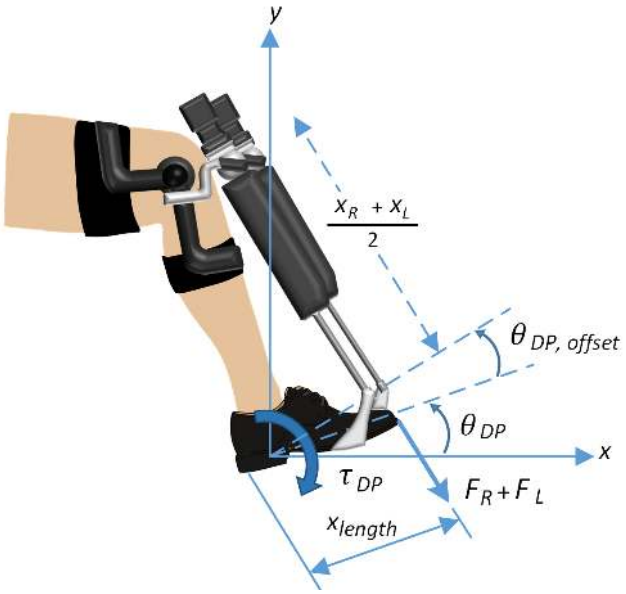

Figure 3: Sagittal plane representation of the Anklebot.
Adapted from **??**).

attachment between the ankle and the robot in the sagittal plane. The torque τ_{DP} and the ankle angles $\theta_{DP,offset}$ and θ_{DP} are estimated from a kinematic model of the relationship between the actuator displacement and the ankle angular position.

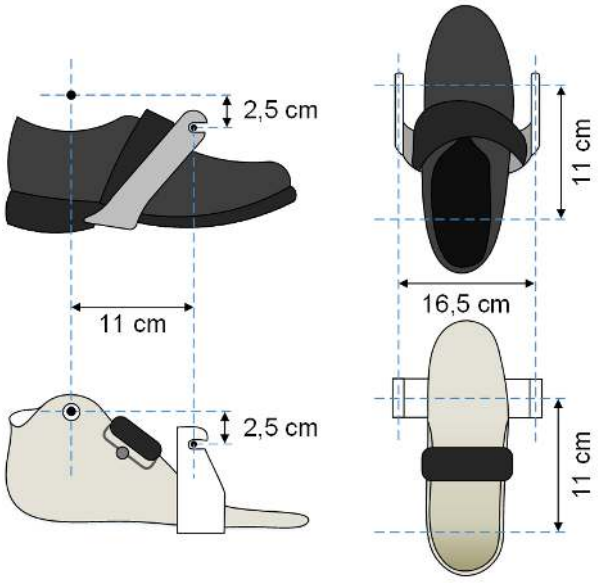

Figure 4: Geometric comparison between Anklebot shoe and customized foot-plate.

When operating the Anklebot, the shoe introduces inertia components and gravitational forces that affect the torque estimation algorithms. Therefore, the shoe was replaced with a orthotic foot-plate, this solution not only allows to release the torque estimation from an

extrinsic load, but also reduce the physical effort done by the user to move his ankle. 3D printed brackets were designed for the foot-plate and coupled considering the geometric relation between the ankle joint and the end effector of the Anklebot (see Figure 4).

3.2 Anklebot Impedance Control

The Anklebot uses a strategy called impedance control which is an approach that establishes a dynamic relation between the force exerted by the actuator and its velocity. In according with (**??**), the dynamic physical interaction of a robot device with its environment can be seen as admittance functions, $(Y(s))$, which accepts force inputs and yield motion outputs, or impedances functions, $(Z(s))$, which accepts motion inputs and yield force outputs. These two concepts are frequently regarded as equivalent and interchangeable representations of the same system.

$$Y(s) = \frac{F(s)}{V(s)} \quad \text{and} \quad Z(s) = \frac{F(s)}{V(s)} \tag{3.3}$$

In Equation 3.3, $F(s)$ and $V(s)$ refers to force and motion functions respectively.

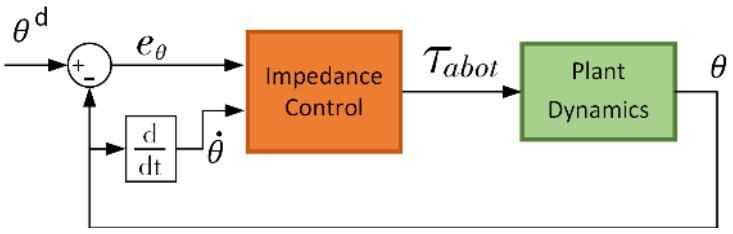

Figure 5: Schematic representation of the Anklebot Impedance control.

Figure 5 shows the impedance control system of the Anklebot, in this, the plant dynamics block represents an admittance function that can be represented as a second order system:

$$Y(s) = \frac{1}{I_{abot}s^2 + B_{abot}s}, \tag{3.4}$$

where I_{abot}, B_{abot} are the inertia and damping of the Anklebot respectively.

To accomplish determined desired trajectory of the Anklebot (θ^d), the impedance control block regulate its torque (τ_{abot}) according to a linear combination of position error and velocity in the form:

$$\tau_{abot} = \underbrace{(\theta^d - \theta)}_{e_\theta} K_v + \dot{\theta} B_v, \tag{3.5}$$

where θ^d and θ are the desired and angular position, e_θ is the position error, the term K_v is called virtual stiffness and describes the relationship between the torque exerted by the

actuator and its angular position, and the term B_v is called virtual damping and describes the relationship between the torque exerted and the angular velocity.

3.3 Ankle/Anklebot inverse dynamic model

The ankle torque estimation approaches proposed in this thesis are designed to be implemented in the Anklebot robot, they require an inverse system model that involves both the ankle and robot dynamics.

Since the Ankebot was delimited to operate in dorsi-plantar flexion, its degree of freedom becomes $n = 1$ and the inverse dynamic model for the ankle-Anklebot system is given by:

$$I_{ankle+abot}\ddot{\theta}_{DP} + B_{ankle+abot}\dot{\theta}_{DP} + \tau_G(\theta_{DP}) + \tau_{fric}\left(\dot{\theta}_{DP}\right) = \tau_{abot} + \tau_{ankle} \tag{3.6}$$

In comparison with (2.1), $M(\theta)$ and $C(\dot{\theta}, \theta)$ were reduced to a scalar inertia (I) and a damping (B) components, the subscript $_{ankle+abot}$ refering to the combination between the ankle and robot dynamics, $\tau_G(\theta_{DP})$ represents the gravitational torque due to the ankle and shoe weight, τ_{abot} is the torque provided by the actuator (τ_{DP} in Equation (3.1)) and τ_{ankle} is the ankle active torque considered as a disturb.

3.3.1 Experimental identification of the Anklebot friction torque

Although the Anklebot is a backdrivable robot, during its operation was observed a frictional force that opposes the movement of the linear actuators and that varies with the speed, then, a torque, τ_{fric}, product of that force was included in the model. Therefore, a function describing τ_{fric}, based on (**????**) is presented here.

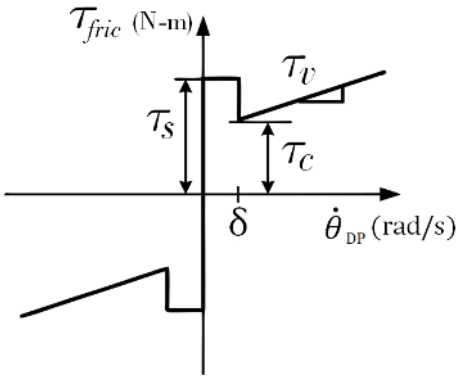

Figure 6: Proposed model for Anklebot friction. Font: **??**)

In figure 6 is depicted the selected model for τ_{fric}, where δ is the boundary lubrication velocity. The friction torque is modeled as a nonlinear function including static (τ_s),

Coulomb (τ_c), and viscous friction (τ_v):

$$\tau_{fric}(\dot{\theta}_{DP}) = \begin{cases} \tau_s & \text{if } \dot{\theta}_{DP} \leq \delta \text{ and } |\tau_{abot}| < \tau_s \\ \tau_c \ \ sgn(\dot{\theta}_{DP}) & \text{if } \dot{\theta}_{DP} \leq \delta \text{ and } |\tau_{abot}| \geq \tau_s \\ \tau_c \ \ sgn(\dot{\theta}_{DP}) + \tau_v \ \ \dot{\theta}_{DP} & \text{otherwise} \end{cases} \tag{3.7}$$

An experimental procedure based on **??**) is reproduced here to measure the frictional components described in Equation 3.7, for this, an open-loop control was implemented on the Anklebot to drive the ramp signal :

$$\tau_{abot}(t) = m\,t, \quad t > 0 \tag{3.8}$$

where t denotes the time and $m > 0$ is the ramp slope. Figure 7b is shows the commanded Anklebot torque for a configured slope $m = 10$ N-m/s, and Figure 7a the corresponding angular velocity.

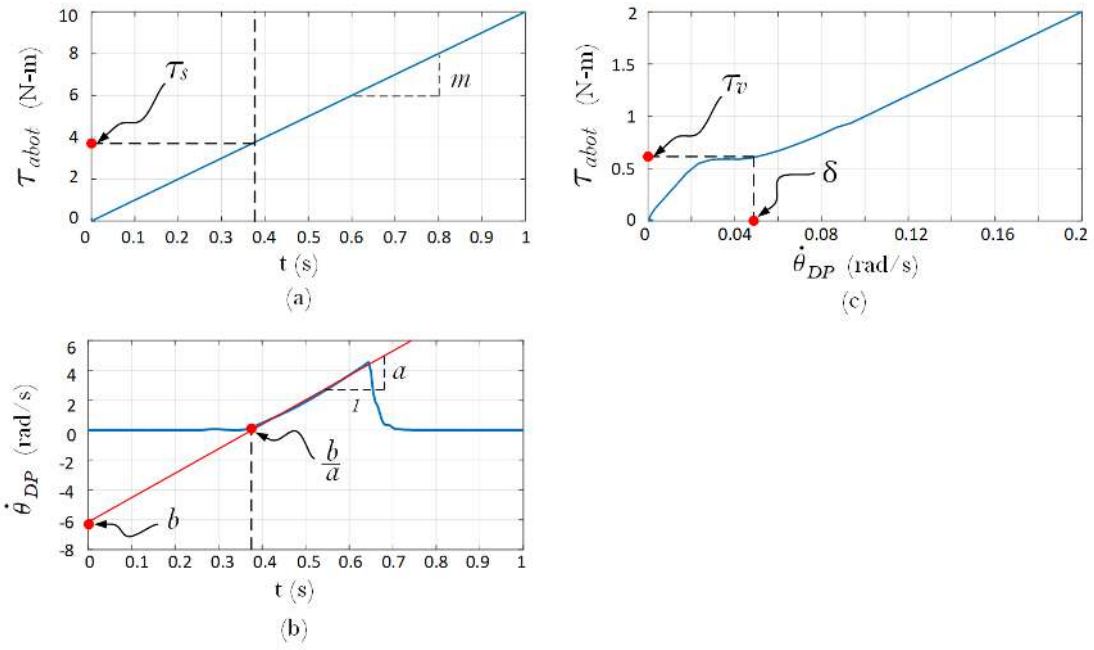

Figure 7: Friction parameter characterization. (a) The Anklebot was commanded to track a ramp reference, (b) when torque achieve the static friction, the velocity actuator begins to increase linearly, the key features b, a/b and $a/1$ are to calculate identified to calculate τ_v and τ_c. (c) The boundary lubrication velocity, δ, is calculated graphically by looking the angular velocity when τ_v begin.

A linear model was superimposed to fit with the angular velocity data (red line in Figure 7a), its slope, as well as the asymptotes that intercept with $\dot{\theta}$ and time axis, are used to

compute the viscous and coulomb parameters:

$$\tau_v = \frac{m}{a} = \frac{10 \text{ N-m/s}}{16.36 \text{ rad/s}^2} = 0.61 \frac{\text{N-m s}}{\text{rad}} \tag{3.9}$$

and

$$\tau_c = \frac{b}{a} m = \frac{6.158 \text{ rad/s}}{16.36 \text{ rad/s}^2} 10\text{N-m/s} = 3.76 \text{ N-m} \tag{3.10}$$

the static friction component (τ_s) is calculated as the torque at moment when the velocity is large enough to star moving the end effector (see Figure 7b):

$$\tau_s \approx 3.88\text{N-m}. \tag{3.11}$$

Finally, Figure 7c shows the Anklebot torque in terms of its angular veolcity where the boundary lubrication veolcity can be approximate as $\delta \approx 0.05$ rad/s.

Figure 8 shows the results of an experimental verification of the developed friction model. The procedure consists in control the Anklebot angular displacement to follow a desired reference $\theta^d_{DP}(\text{degrees}) = 10\sin(2\pi f t)$, with $f = 0.25$ Hz. The corresponding controller is a PD control with programmed gains of $K_v = 90$ N-m/rad and $B_v = 5$ N-m-s/rad for virtual stiffness and damping respectively. As can be seen the friction torque (bottom plot) alternates between an approximate range of [4 -4] N-m, these values are nearly close to the static friction. Notice that when the angular velocity overcomes the lubrication boundary velocity (red box in angular velocity plot), the friction torque has a stick-slip behavior(zoom circle in friction torque plot) which is an effect of the viscous component.

Notice that at low velocities the friction torque cannot be identified with accuracy, that is because a formulation of the stribeck effect was no considered for the friction model. Nevertheless, the developed model can be considered a close approximation to the real friction torque presented in the actuator.

3.4 Ankle/Anklebot inverse dynamic model identification: a case study

The ankle/Anklebot inverse dynamic model (Equation 2.1) depends of the variation of ankle and Anklebot mechanical impedance parameters. The inertia, damping and stiffness components of ankle impedance varies from user to user, thus, the estimation approaches will require to identify the inertia and damping of the compound ankle/Anklebot system, i.e., $I_{ankle+abot}$ and $B_{ankle+abot}$, as well as the gravitational torque τ_G for any user wearing the Anklebot before estimating the ankle torque.

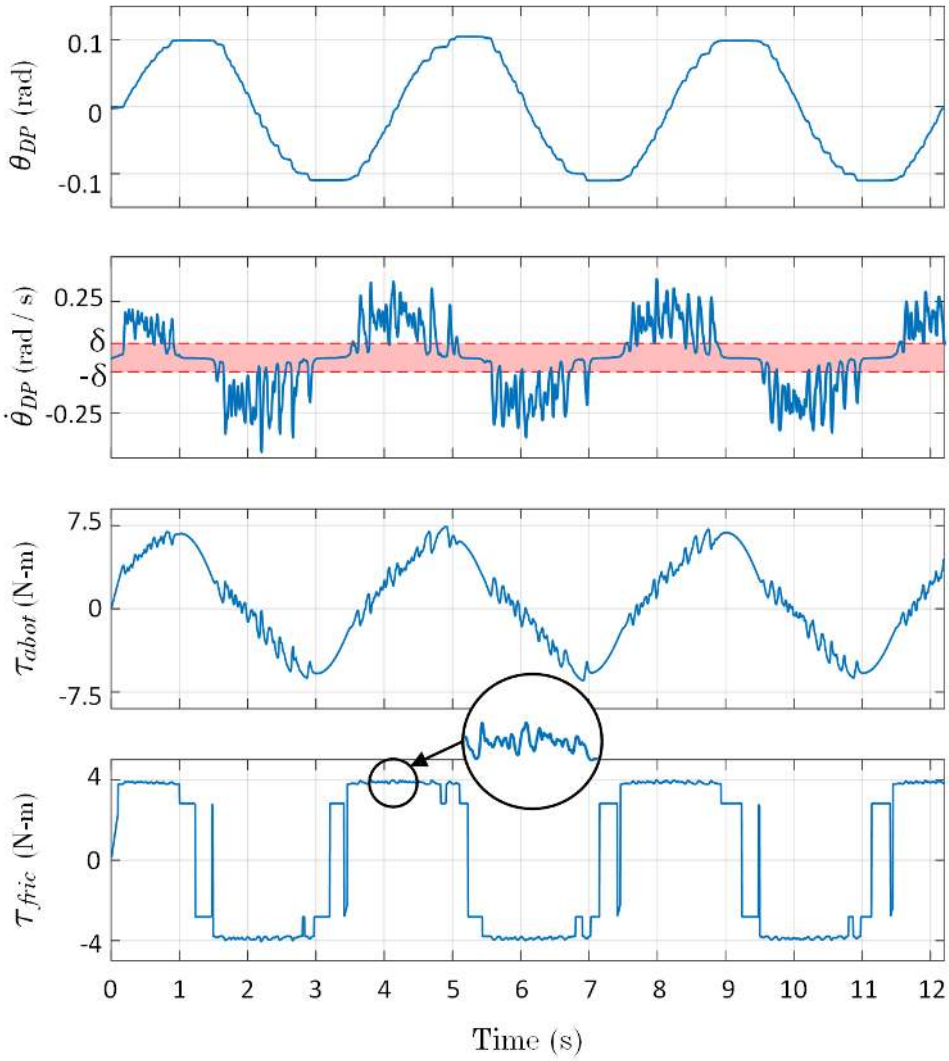

Figure 8: Friction time responses.

This section develops the ankle-Anklebot system identification for a case study, consisting in a voluntary subject without neuromuscular disorders wearing the Anklebot. The resulting ankle/Anklebot system will be the used for the ankle torque estimation experiments described in chapter 5 (page 49).

3.4.1 **Passive Ankle Impedance and Anklebot dynamics**

For identification of the dynamic plant formed by the Passive Ankle Impedance (when subject does not performs muscle activation) and the Anklebot, an experiment based on the described in section 3.4 of **??**) is carried out on the Anklebot, the subject is instructed to relax its muscles while the Anklebot control his ankle movement. The control system maintains the foot in a 0° reference when a random torque perturbation signal (in DP flexion) with ± 7.7 N-m of amplitude and 100 Hz of bandwidth is applied during 60 seconds (see Figure 9). The impedance control was programmed with $K_v = 5$ N-m/rad

(virtual stiffness) and $B_v = 0$ N-m-s/rad (virtual damping).

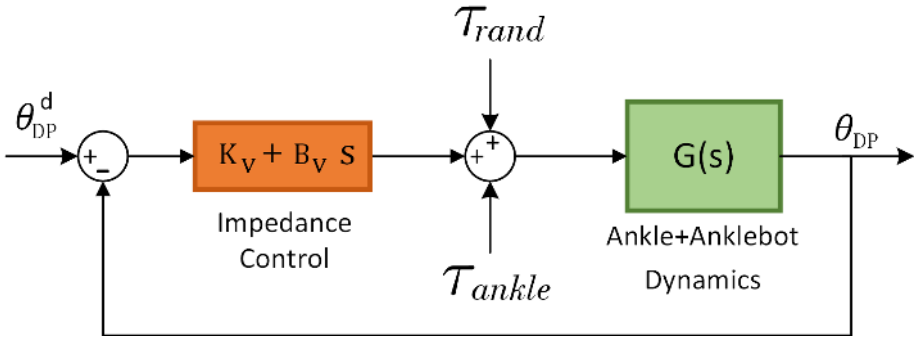

Figure 9: Control block diagram for Ankle/Anklebot Dynamics identification. Adapted from **??**).

The ankle/Anklebot dynamics can be expressed by the admittance function:

$$G(s) = Y_{ankle+abot}(s) = \frac{1}{I_{ankle+abot}s^2 + B_{ankle+abot}s + K_{ankle}}, \tag{3.12}$$

where the term K_{ankle} refers to the ankle joint stiffness. Notice that due to the back-driveability property, the stiffness actuator is neglected. The closed-loop transfer function between random torque perturbations to the actuator (τ_{rand}) and the corresponding angular displacement (θ_{DP}) is represented as:

$$\begin{aligned} Y_{CL}(s) = \left.\frac{\theta_{DP}(s)}{\tau_{rand}(s)}\right|_{CL} &= \frac{Y_{ankle+abot}(s)}{1 + (K_v + B_v s)Y_{ankle+abot}(s)} \\ &= \frac{1}{I_{ankle+abot}s^2 + (B_{ankle+abot} + B_v)s + (K_{ankle} + K_v)} \end{aligned} \tag{3.13}$$

and the corresponding closed loop mechanical impedance:

$$Z_{CL}(s) = Y_{CL}^{-1}(s) = I_{ankle+abot}s^2 + (B_{ankle+abot} + B_v)s + (K_{ankle} + K_v) \tag{3.14}$$

After developing the control experiment, the random input torque and the resulting angular trajectory were recorded to generate a response in the frequency domain of the closed-loop transfer function described in (3.13). Figure 10 shows the corresponding frequency response of Equation 3.13, it was obtained by using the MATLAB's *tfestimate* function. Such a function is based on the Welch's averaged periodogram method which consists in broke the input and output signals into sections or data blocks, and then compute the averaged periodograms (the estimate of the spectral density of the signal) of each section. The coherence of the estimated transfer function presented considerable variability (see bottom plot in Figure 10), nevertheless, up to the 6 Hz frequency it exhibit averaging values about 0.81 which satisfy the frequency range of interest for studies of the biomechanics of the ankle (**??**).

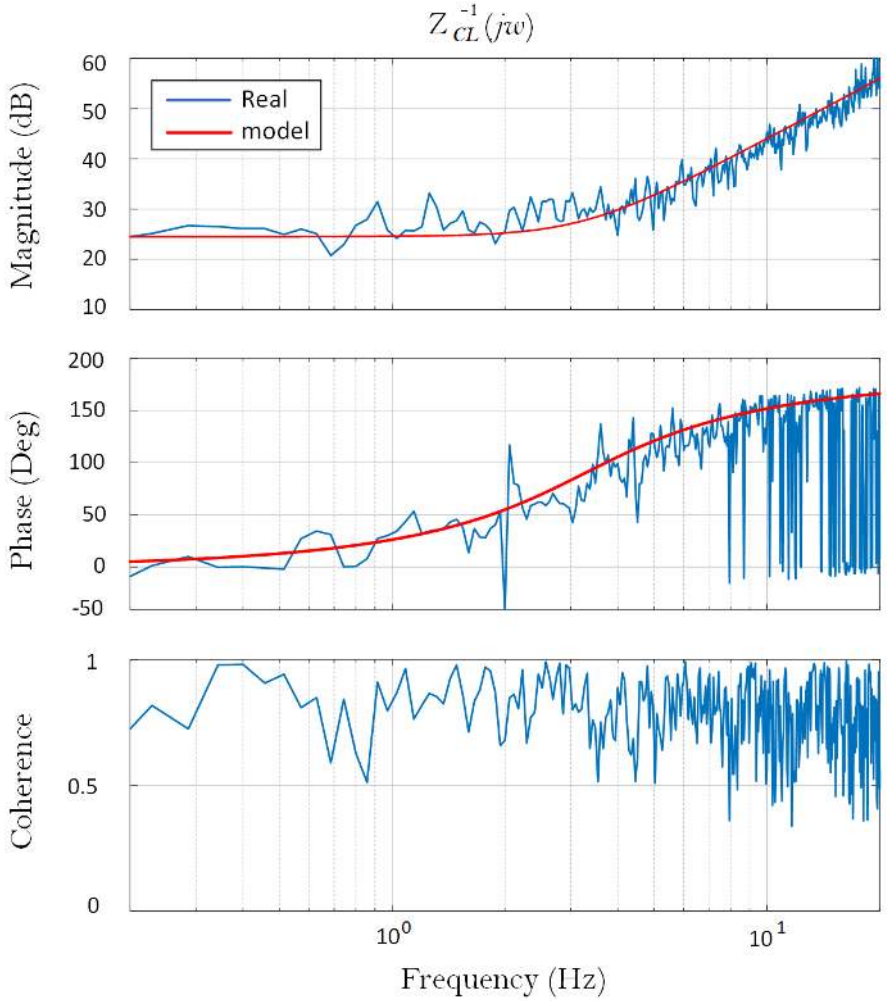

Figure 10: Frequency Response Estimation of the closed-loop mechanical impedance for the ankle/Anklebot system

At low frequencies the impedance magnitudes approach to constant asymptotes, its DC amplitudes represent the stiffness of the systems. An approximate value for the ankle-Anklebot system was 16.807 N-m/rad (24.51 dB), then by subtracting the stiffness control gain (K_v), the ankle stiffness (K_{ankle}) was estimated as 11.807 N-m/rad. This value is consistent with the ankle stiffness under relaxed muscles conditions founded in (**??**).

Once the stiffness was defined, a linear second order model was superimposed for the mechanical impedance response (dashed lines in magnitude and phase plots in Figure 10). In order to fit with the frequency function estimation, the parameters values of the linear second order model was adjusted taking into account the damping and inertial ranges of the ankle founded in (**??**). The resulting values that best fit with $I_{ankle+abot}$, $B_{ankle+abot}$ and K_{ankle} were 0.04 kg-m^2, 1.992 N-m-s/rad and 29.78 N-m/rad respectively. This values are in concordance with data founded in the literature (**??????**).

3.4.2 Gravitational Torque

The torque τ_G is defined as the moment due to the gravitational forces (see Figure 11), its magnitude is calculated as the moment arm l times the tangential component of the weight vector $\mathcal{M}\ g$ located at the center of mass ($c.m.$):

$$\tau_G(\theta_{DP}) = l\ \mathcal{M}\ g\ \cos(\theta_{DP}) \tag{3.15}$$

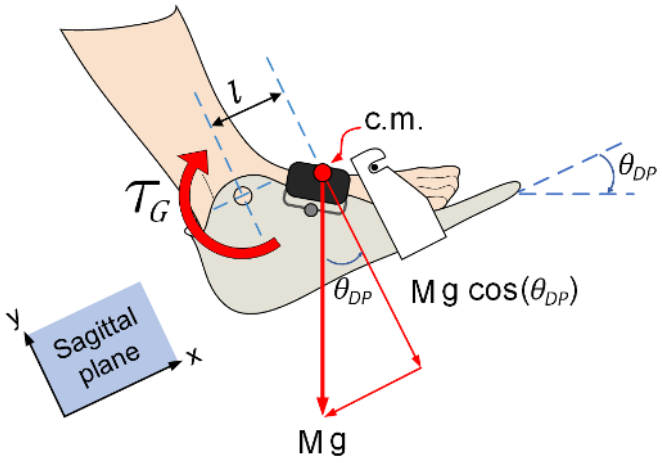

Figure 11: Free-body diagram of the set ankle and foot-plate.

where $\mathcal{M}$ is the mass combination of the ankle and foot-plate, g is the acceleration due to gravity and l is the length (in the sagittal plane) from the ankle joint to the center of mass of the set ankle-foot-plate . In according with **??**) the foot mass is calculated by $m_{foot} = 0.0145 \cdot m_T$, where m_T is the total mass of human body, the ankle center of mass in the x-axis is calculated as 50 % of the foot length, namely $x_{foot} = 0.5\, l_{foot}$. The foot-plate weighs 0.272 kg (m_{fp}) and its center of mass in the x-axis (x_{fp}) is 0.047 m from the center of rotation.

The equivalent mass (M) and moment arm l for the ankle-foot-plate set are:

$$\begin{aligned} \mathcal{M} &= m_{fp} + m_{ankle}, \\ l &= \frac{m_{fp}\ x_{fp} + m_{foot}\ x_{foot}}{\mathcal{M}}. \end{aligned} \tag{3.16}$$

Table 1 contains a calculation of $\mathcal{M}$, m_{foot}, l and x_{foot} with $l_{foot} = 0.253$ m and $m_T = 68$ kg. For the coming implementation of the estimator approaches on the mock-up/Anklebot system, it will be necessary to modify the gravitational torque components to $\mathcal{M} = m_{fp}$ and $l = x_{fp}$.

Table 1: Anthropometric data for the ankle-foot-plate set

m_{foot}	x_{foot}	$\mathcal{M}$	l
0.986 kg	0.1265 m	1.258 kg	0.0505 m

4 EXPERIMENTAL VALIDATION

In this chapter, the above mentioned torque estimation approaches are implemented on the Anklebot and tested with an physical mock-up assembled to replicate the human ankle movement in the sagittal plane. The experimental setup objective is to estimate the external torque transmitted from the mock-up to the Anklebot, this torque can be measured with a load cell incorporated to the mock-up. The estimated torques are expected to be equal to the measured one.

For the Anklebot control system, the external torque can be considered as a disturbance input, the algorithms were programed on the Anklebot to estimate this disturbance torque (see Figure 12). However, since compensation is out of scope, the disturbance estimation is not feedback into the control strategy, and the algorithms operate simultaneously without affecting the control system operation. Two tests are realized with this experimental setup. The former is to tune the parameters of each approach in order to yield a proper estimation. In this, the impedance control is programmed with fixed parameters to track a sinusoidal reference for the Anklebot. The latter allows a performance assessment of the estimated torques, for which, the impedance control is programmed too with a sinusoidal reference but with variable parameters.

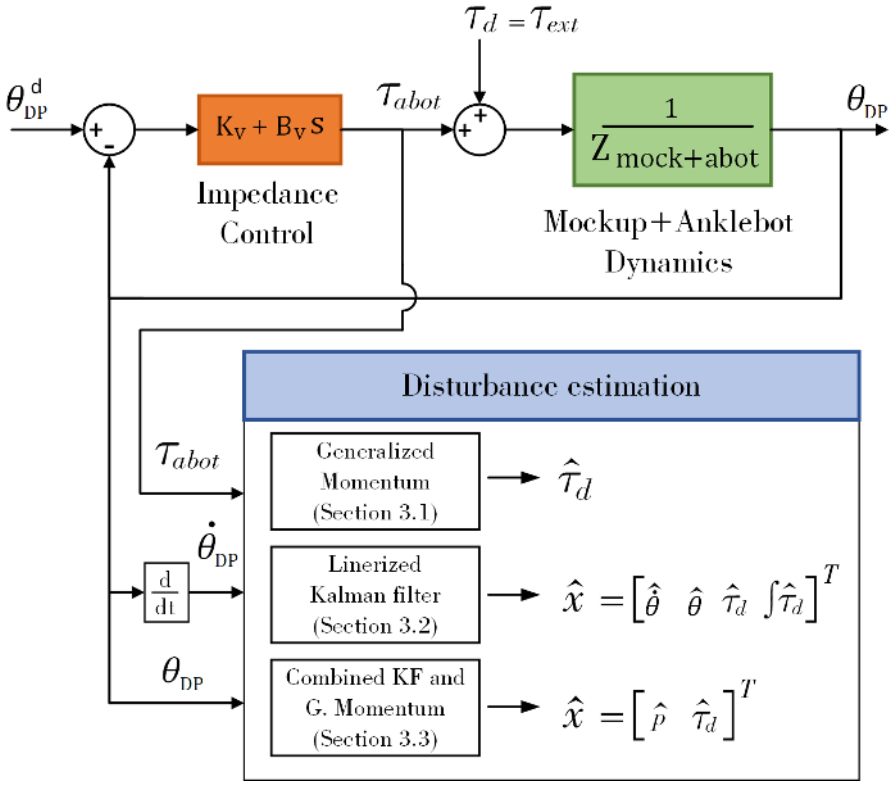

Figure 12: Schematic diagram of the experimental setup

The physical mock-up is composed by an Ankle Foot Orthosis (AFO) and an spring coupled on its backside, this device is equipped with a load cell (see Figure 13a) that measures the force produced by the extension and compression spring forces product of the dosriflexion and plantarflexion respectively. The leg brace and foot-plate of the AFO are linked by a common hinge joint (see Figure 13b) that allows a dorsiflexion and plantarflexion as the ankle joint. The foot-plate is practically the same designed in section 3.1 but with a 3D-printed support added on its back to place the load cell. The mock-up is attached to the Anklebot conserving the same geometrical relation as in Equation (3.1) which guarantees a complete transmission of the actuator torque.

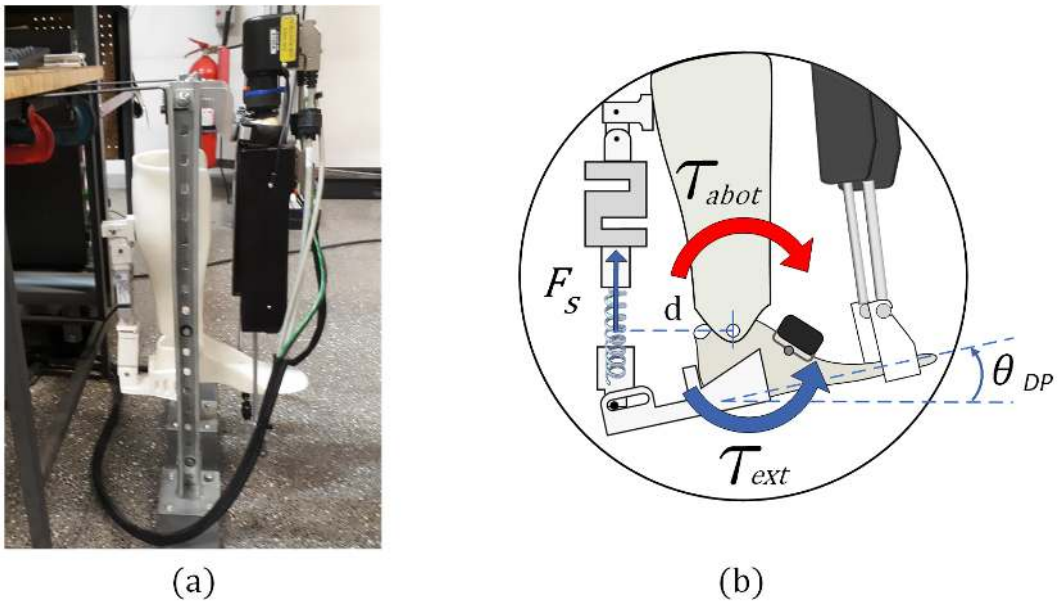

Figure 13: Physical mock-up to validate the torque estimation.

When the Anklebot moves the foot-plate, a spring positioned before the load cell compress or extends generating a force that is parallel to the orthosis axis (Figure 13b). The spring force (F_s) is then measured by the load cell and converted to torque (τ_{ext}) by:

$$\tau_{ext} = F_s \cdot d, \tag{4.1}$$

where $d = 0.15$ m is the perpendicular distance from F_s to the axis of rotation. The load cell was calibrated by applying compression and extension forces corresponding to known weight masses loaded on the sensor, then a data acquisition system amplify and register the voltage output signals (Figure 14a). By doing a linear regression (see Figure 14b) of the data sensor, a function describing the force sensor measurement (in Newtons) in terms of the voltage (in volts), $F_s(V)$, was obtained as:

$$F_s(v) = 48.577 \cdot V - 97.487, \tag{4.2}$$

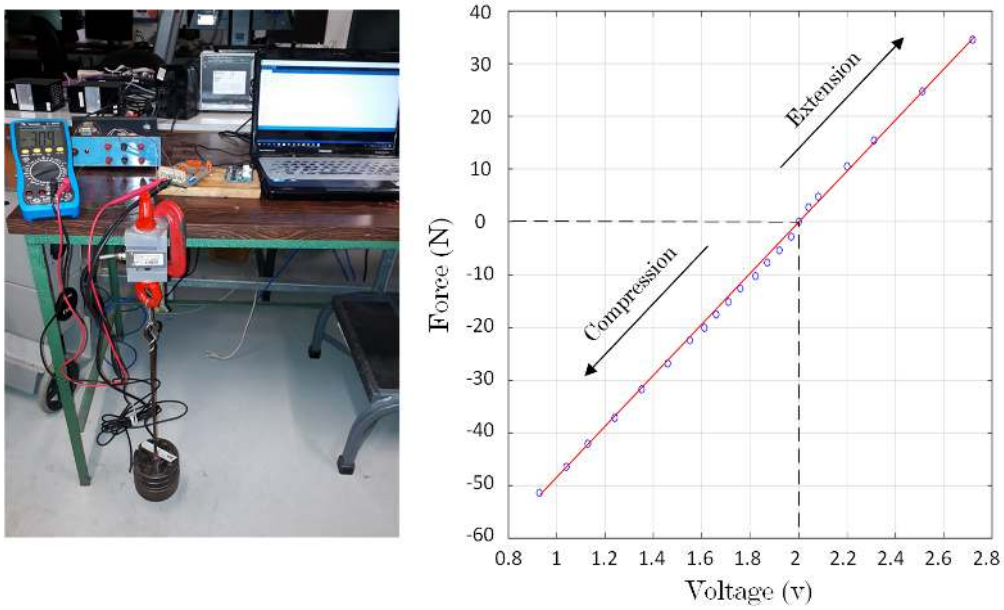

(a) (b)

Figure 14: Load cell characterization.

4.1 Mock-up and Anklebot dynamics

The dynamic model of the mock-up/Anklebot system is given by:

$$I_{mock+abot}\ddot{\theta}_{DP} + B_{mock+abot}\dot{\theta}_{DP} + \tau_G + \tau_{fric} = \tau_{abot} + \tau_{ext} \tag{4.3}$$

where the subscript $mockup + abot$ refers to the combination of the mock-up and robot dynamics, τ_{ext} is the same torque described in Equation (4.1).

In the same way as Equation 3.14, a closed-loop transfer function describing the mechanical impedance of the mock-up/Anklebot system can be defined:

$$Z_{CL}(s) = I_{mock+abot}s^2 + (B_{mock+abot} + B_v)s + (K_{mock+abot} + K_v) \tag{4.4}$$

The same procedure described in section 3.3.1 was carried out to obtain a frequency response of the close-lop transfer function representing the mechanical impedance of the mock-up/Anklebot system. Figure 15 shows the frequency response obtained for equation 4.4, blue lines represent the estimated data from the Power spectral density analysis and red lines represent a second-order transfer function model whose parameters were adjusted in order to approach with real data. As can be seen in the magnitude plot, at low frequencies it can be observed an approximated value of 17.15 dB, this value corresponds to 7.2 N-m/rad which is the sum of stiffness quantities $K_{mock+abot} + K_v$. Since K_v was previously programed as 5 N-m/rad, it can be subtracted from 7.2 N-m/rad to obtain

$K_{mock+abot} = 1.2$ N-m/rad which corresponds the spring stiffness. The parameters $I_{mock+abot}$ and $B_{mock+abot}$ were calculated as 0.0281 kg-m^2 and 0.761 N-m-s/rad respectively, these values are close to the found in (**??**).

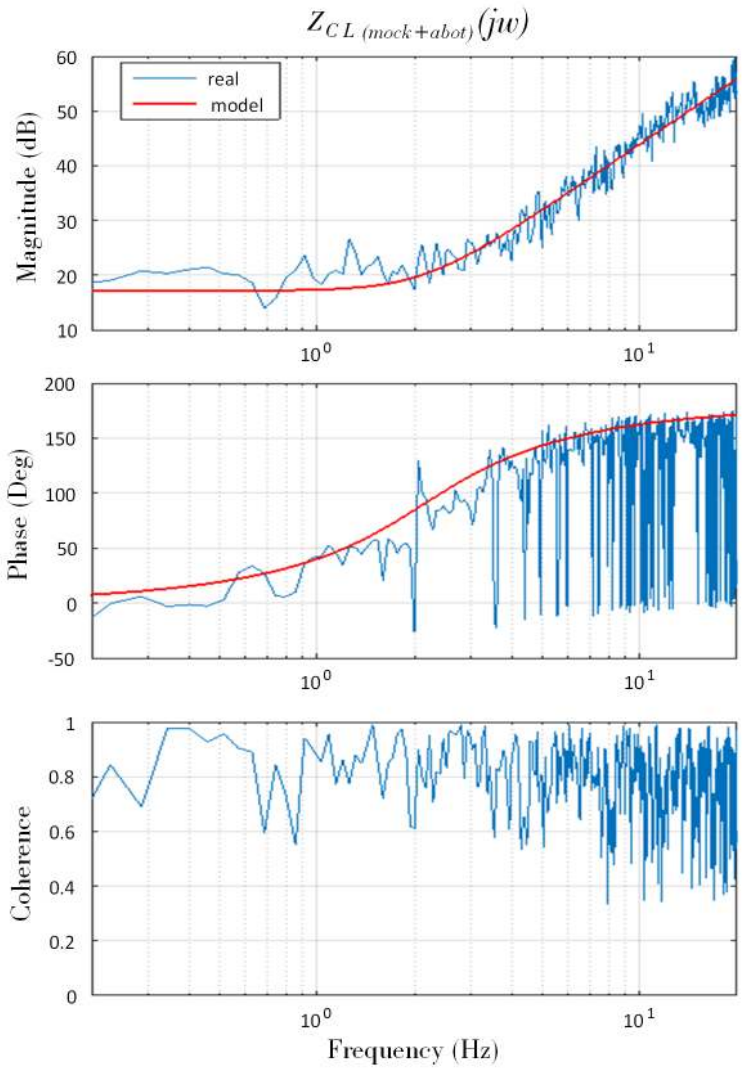

Figure 15: mock-up/Anklebot mechanical impedance in frequency domain. It is a frequency response estimation of the closed-loop transfer function of equation 4.4.

As expected, for all frequencies the magnitude response for equation 4.4 was smaller than that of the ankle/Anklebot system.

4.2 Test 1: Tuning of estimators parameters

The first of the two tests was performed in order to adjusts each estimation approaches, to this, the impedance control was configured with $K_v = 90$ N-m/rad and $B_v = 5$ N-m-s/rad constant gain parameters and commanded to track a sinusoidal reference with amplitude and frequency equal to 0.174 radians (10 degrees) and 0.25 Hz respectively, during 12

seconds. Figure 16 shows the time responses for Test 1, as can be seen , the angular position is not totally reached, this is because the mechanical impedance properties of the mock-up/Anklebot system, especially its stiffness . The bottom plot shows the torque provided by the Anklebot and the measured by the load cell, this latter represents the disturbance torque to be estimated by the algorithms.

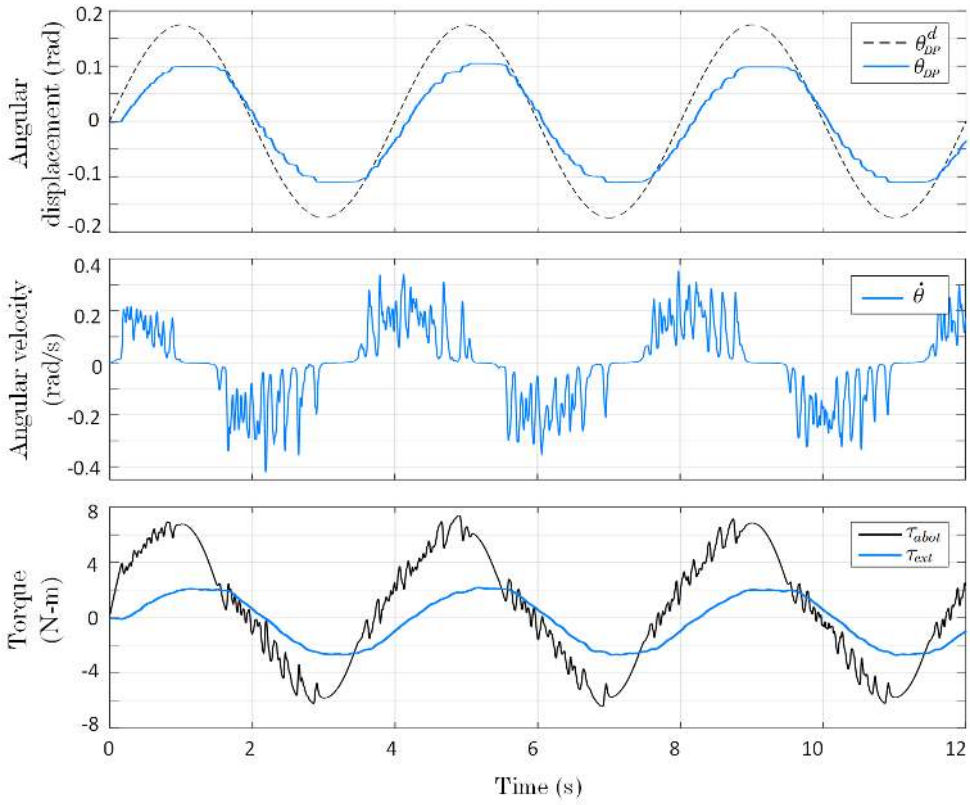

Figure 16: Time responses of the impedance control for Test 1. Top: Reference trajectory (dashed line) and angular displacement (blue line). Middle: Angular velocity. Bottom : Atuator torque (black line) and external torque (blue line).

4.2.1 **Generalized momentum approach**

In Figure 17 is shown the time response of the estimated disturbance torque, $\hat{\tau}_d$, obtained by the generalized momentum. As can be seen, the resulting r signal is a smoothed version of $\hat{\tau}_d$, which is in concordance with the explained in section 2.1. During the implementation it was observed that adjusting K_I implies in a compromise between amplitude and phase of the filtered signal r, i.e., the higher the observer gain, the closer in phase is r with respect to τ_{ext}, and conversely. Taking into account the above, for Test 1 the generalized momentum approach was tested with two observer gain values set heuristically as $K_I = 4$ and $K_I = 0.85$ to see which parameter is more accurate in the external torque estimation.

Figure 18 shows the torque estimation results considering these two observer gains compared with the external torque. Whereas for $K_I = 4$ (red dashed line), r showed to be very close in phase but distant in amplitude with respect to τ_{ext} (blue line), for $K_I = 0.85$ (green

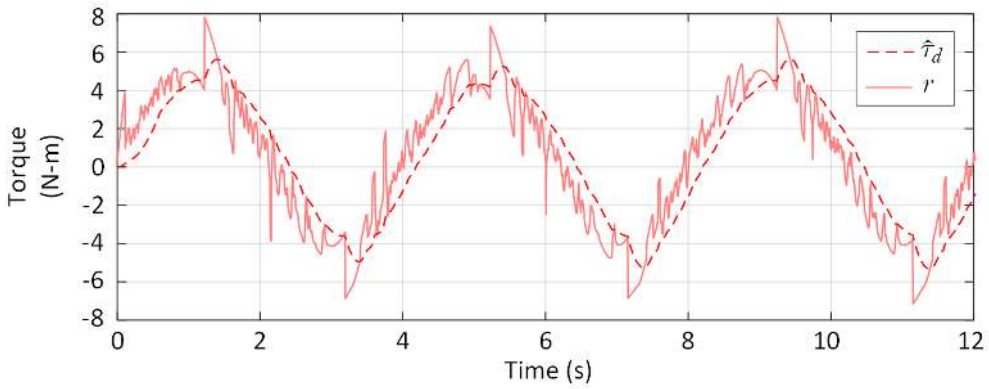

Figure 17: Disturbance torque estimation by the generalized momentum approach. Red continuous line: Estimated torque. Red dashed line: filtered signal.

dashed line) r was closer in amplitude but with a considerable time lag of 0.35 seconds on the left and 0.75 seconds on the right with respect to τ_{ext}.

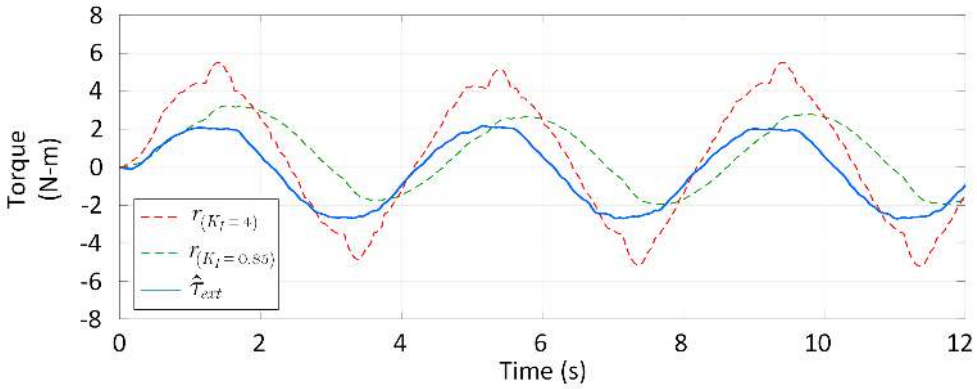

Figure 18: Torque estimation obtained by the generalized momentum approach. A greater $K_I = 4$ gain produces a r signal that is close in phase but a higher amplitude than τ_{ext}, conversely, a lesser $K_I = 0.85$ gains produces a greater time lag and a better adjusted amplitude with respect to τ_{ext}.

4.2.2 **Linearized Kalman filter approach**

The discrete Kalman filter implementation require the Mock-up/Anklebot model (Equation 4.3 on page 39) to be represented as an state space augmented system in the form:

$$\begin{bmatrix} \ddot{\theta} \\ \dot{\theta} \\ \dot{\hat{\tau}}_d \\ \dot{\hat{\tau}}_d \end{bmatrix} = \underbrace{\begin{bmatrix} \frac{-B_{mock+abot}}{I_{mock+abot}} & \frac{-\tau_G}{I_{mock+abot}} & \frac{-1}{I_{mock+abot}} & 0 \\ 0 & 0 & 0 & 0 \\ 0 & 0 & 0 & -\omega_0^2 \\ 0 & 0 & 1 & 0 \end{bmatrix}}_{A_c} \underbrace{\begin{bmatrix} \dot{\theta} \\ \theta \\ \hat{\tau}_d \\ \int \hat{\tau}_d \end{bmatrix}}_{x} + \underbrace{\begin{bmatrix} \frac{1}{I_{mock+abot}} \\ 0 \\ 0 \\ 0 \end{bmatrix}}_{B_c} \underbrace{(\tau_{abot} - \tau_{fric})}_{u}, \tag{4.5}$$

with output equation:

$$y = \underbrace{\begin{bmatrix} 1 & 0 & 0 & 0 \\ 0 & 1 & 0 & 0 \end{bmatrix}}_{H} \underbrace{\begin{bmatrix} \dot{\theta} \\ \theta \\ \tau_d \\ \int \tau_d \end{bmatrix}}_{x}. \tag{4.6}$$

Notice that the gravitational torque τ_G (Equation 3.15 on page 34) is the only non-lineal component, thus, linearization of A_c just required the partial derivative:

$$\left.\frac{\partial \ddot{\theta}}{\partial \theta}\right|_{\theta=\theta^k} = -\frac{1}{I_{mock+abot}} \frac{\partial(\tau_G)}{\partial \theta} = \frac{\mathcal{M} g l sin(\theta)}{I_{mock+abot}} \tag{4.7}$$

After linearizing, A_c and B_c were discretized by using $A_k = I + A_c T_s$ and $B_k = T_s B_c$ respectively, with time sample $T_s = 0.5$ ms. The linearization and therefore the discretization are computed iteratively before the Kalman filter execution.

The covariance matrices for the process and measurement noise were adjusted as:

$$Q = diag\{0.01,\ 0.01,\ 0.001,\ 0.0001\} \tag{4.8}$$

$$R = diag\{1e{-}5,\ 1e{-}5,\ 1e{-}5,\ 1e{-}5\} \tag{4.9}$$

In Figure 19 are depicted the process input noises with zero-mean and normal distribution.

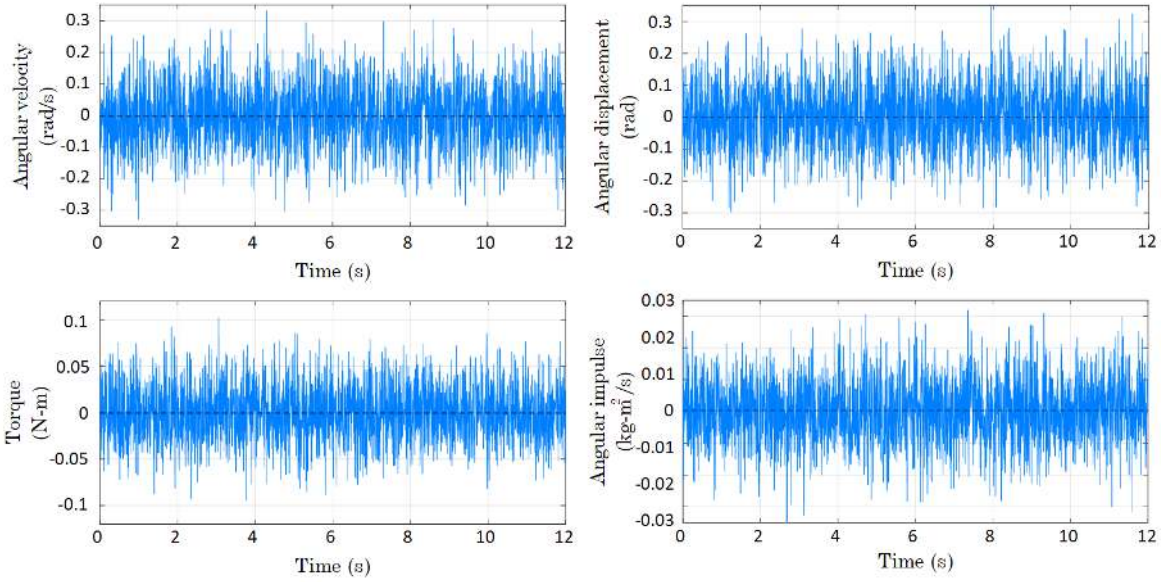

Figure 19: Process input noise for Kalman filter approach

Figure 20 shows the estimated estates of the Kalman filter implementation. Whereas the observable states matched the measured signals (angular velocity on top-left and displacement on top-right), the non-observable states showed certain differences with the

real variables. The estimated torque $\hat{\tau}_d$ (bottom-left) turned out to be in phase with the external torque τ_{ext}. Finally, the estimated integral of the disturbance torque, $\int \hat{\tau}_d$, is showed on bottom-right plot, an off-line numerical integration of the external torque, $\int \tau_{ext}$, was computed to verify the concordance of such estimated estate. Although these two signals conserve similarity, there is a considerable amplitude difference.

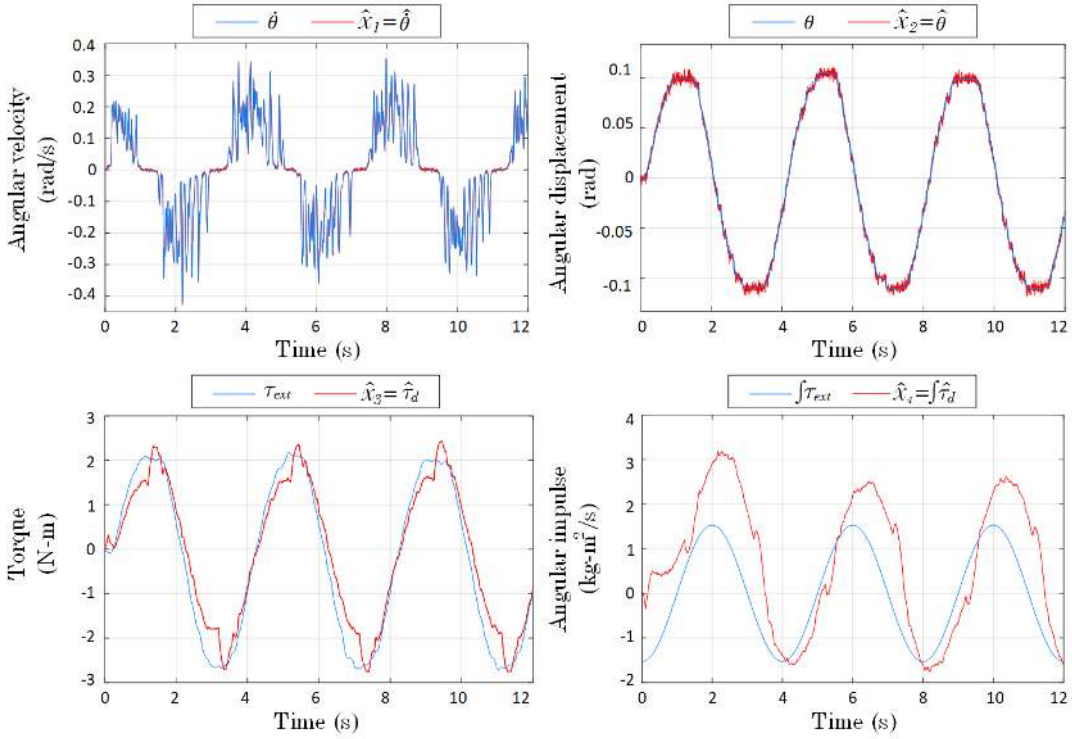

Figure 20: State estimation result for the Kalman filter approach

4.2.3 Combined Kalman and Generalized momentum approach

As explained in section 2.3, the augmented state space model considered for this estimation approach is given by:

$$\underbrace{\begin{bmatrix} \dot{p} \\ \dot{\tau}_d \end{bmatrix}}_{\dot{x}} = \underbrace{\begin{bmatrix} 0 & -1 \\ 0 & A_d \end{bmatrix}}_{A_c} \underbrace{\begin{bmatrix} p \\ \tau_d \end{bmatrix}}_{x} + \underbrace{\begin{bmatrix} 1 \\ 0 \end{bmatrix}}_{B_c} \underbrace{\bar{\tau}}_{u} + w. \tag{4.10}$$

Unlike the Kalman filter approach of section 2.2.2 (page 19), the gravitational torque is considered in the input vector instead of in the state transition matrix, thus, here there is no need of linearization step. The model 4.10 was discretized by using $A_k = I + A_c T_s$ and $B_k = T_s B_c$ and with time sample $T_s = 0.5$ ms.

The covariance matrices for the process and measurement noise were adjusted as:

$$Q = diag\{2.5\text{e}{-5},\ 4.5\text{e}{-5}\} \tag{4.11}$$

$$R = diag\{2\text{e}{-7},\ 2\text{e}{-5}\} \tag{4.12}$$

Figure 21 show the process input noises with zero-mean and normal distribution.

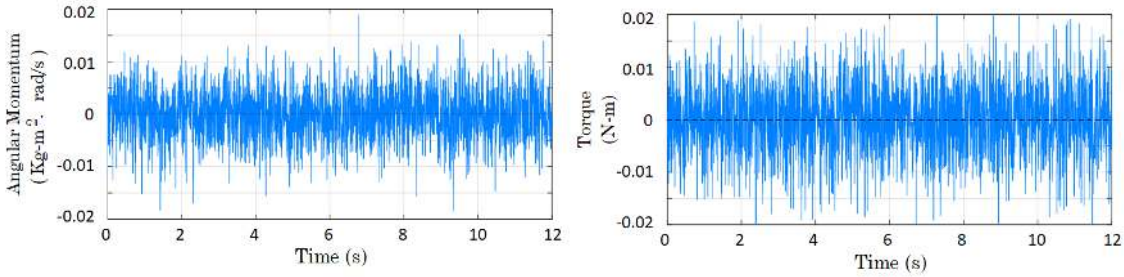

Figure 21: Process input noise for Kalman-based momentum approach

Figure 22 shows the estimated estates in the implementation of the Combined Kalman and Generalized momentum approach. As can be seen, the first estimated state matched the angular velocity signal without much difficulty, this was expected since $\hat{x}_1$ is the observable state.

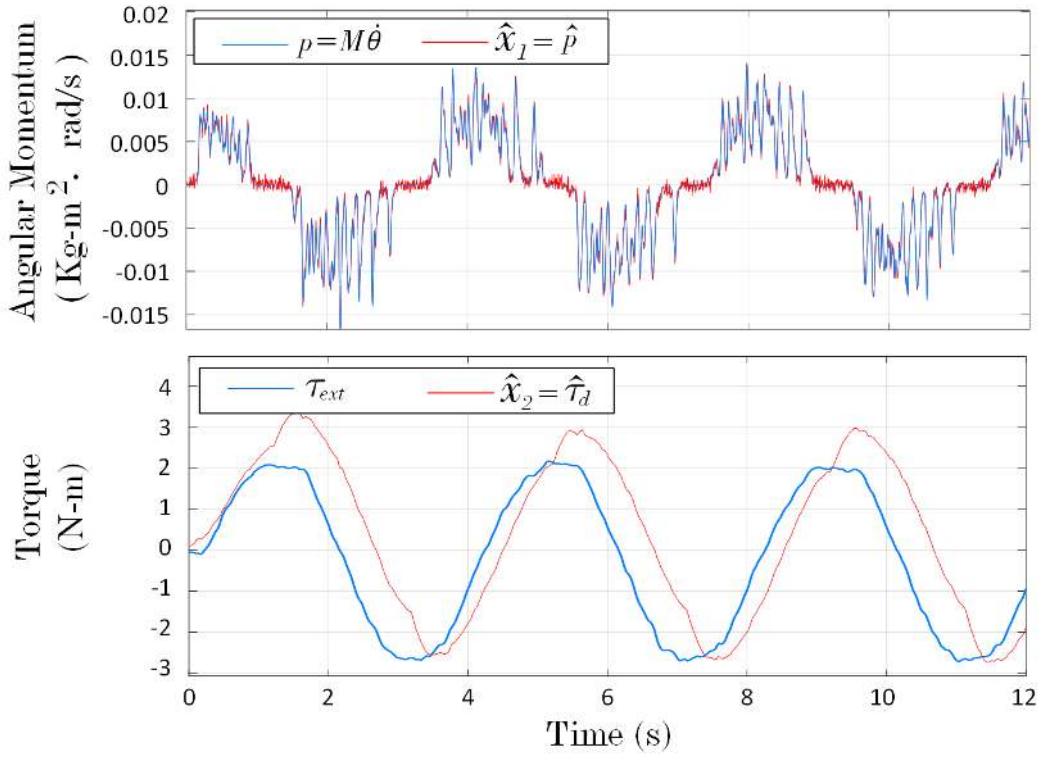

Figure 22: State estimation result for the Combined Kalman and Generalized momentum approach.

The second estimated state (bottom plot) i.e., the torque disturbance estimation, a similar behavior of the discussed in section 4.2.1 for the filtered torque, r, was found. Nevertheless, it showed a closer signal than the generalized momentum approach estimation for the negative, presenting a time lag of 0.25 seconds on the left and 0.53 seconds on the right and peak-to-peak difference of 7.81 N-m.

4.3 Test 2: Performance assessment between estimation approaches

In order to make a comparative analysis of the implemented estimation approaches, a second test in which the impedance control parameters are varied over time is developed here. The purpose of this test is to evaluate the estimation performance when the mock-up/Anklebot system undergoes different input torques. The test is realized in the same experimental setup of Figure 12 (page 37), a sinusoidal reference with amplitude and frequency equal to 0.174 radians (10 degrees) and 0.25 Hz respectively and a duration of 36 seconds was programmed. In contrast with test 1, the K_v parameter of the impedance control was configured to variate over time in according with Table 2.

Table 2: Configuration of test for performance assessment

Phase	Duration (s)	K_v (N-m/rad)
1	[0 12]	30
2	[12 24]	60
3	[24 36]	90

Figure 23 shows the angular displacement (top) and Anklebot torque (bottom) time responses of this experiment. Notice that the greater the K_v parameter is configured, the better the desired sinusoidal trajectory is tracked.

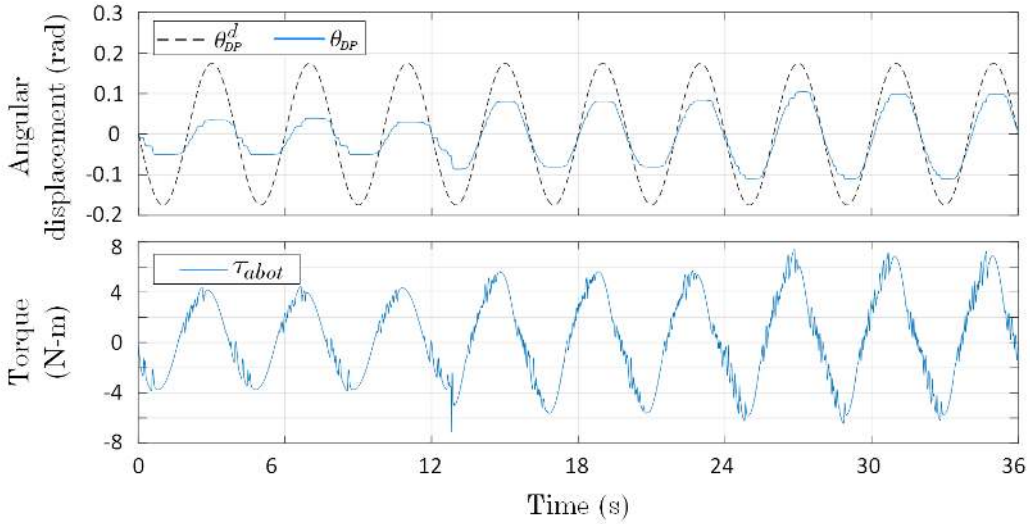

Figure 23: Time responses of test 2. Phase 1: [0 12] (s). Phase 2: [12 24] (s). Phase 3: [24 36] (s).

Figure 24 shows the estimated torques and the measured by the load cell. It can be seen that the three approaches had difficulty in estimating the torque during the first phase, i.e., the first 12 seconds. On the other hand, as soon as the control parameters K_v were increased, the estimation improved for all the approaches. The above mentioned is evidenced in the zoom circles, note that right circle shows a closer tracking of the estimated

torques than the shown in left circle. In all the phases the $\hat{\tau}_d$ achieved by the Kalman filter, approach appears to estimate the load cell torque, τ_{ext}, better than the other two approaches, this is in concordance with the Test 1 results.

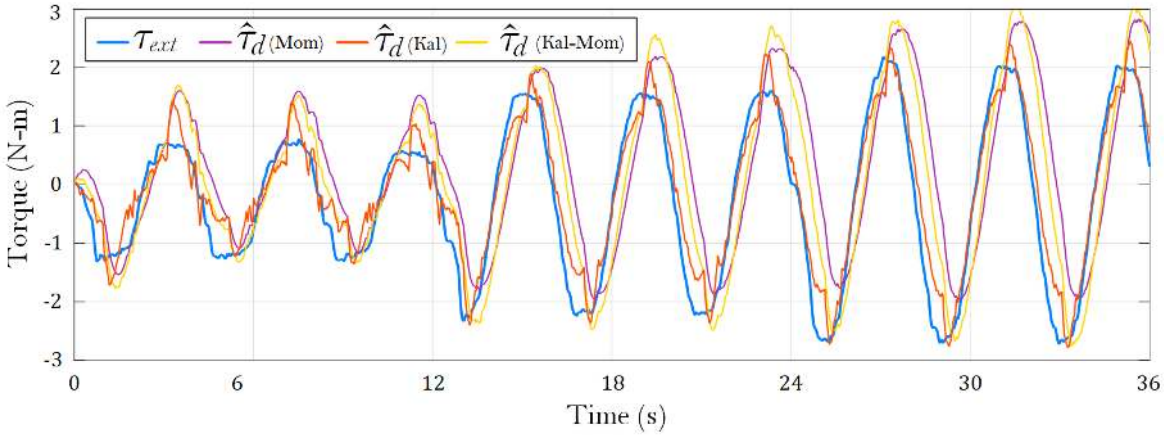

Figure 24: Torque estimation results for test 2. Phase 1 (s): [0 12]. Phase 2 (s): [12 24]. Phase 3 (s): [24 36]. Subscripts ext and d stands for the external and disturbance torques respectively. The abbreviations in brackets Mom and Kal stands for generalized momentum and Kalman respectively.

For quantitative assessment, the root-mean-square error (RMSE) between the estimated disturbance torques and the torque measured by the load cell were calculated by:

$$RMSE = \sqrt{\frac{1}{N}\Sigma_{i=1}^{N}\left(\hat{\tau}_d - \tau_{ext}\right)^2} \tag{4.13}$$

where N is the sample size. Table 3 shows the RMSE calculated separately for each phase of the experiment.

Table 3: Comparison of torque estimation performance

Estimation approach	RMSE (N-m) (phase 1)	RMSE (N-m) (phase 2)	RMSE (N-m) (phase 3)
Generalized momentum	0.6353	1.1960	1.6097
Kalman filer	0.3697	0.3969	0.4052
Kalman based momentum	0.4791	0.9831	1.2149

4.4 Conclusions of experimental validation and outlook

In this chapter, the three proposed approaches for torque estimation have been implemented on an experimental setup consisting in a physical mock-up attached to the Anklebot. This mock-up provided a known external torque to the robot, thus, the purpose of the

experiment was to estimate such known torque. In order to obtain a good dynamic representation of the mock-up/Anklebot system, its inertia and damping were identified by frequency response estimation. Then, the best possible estimated torque was obtained for each approach by tuning its parameters.

The results of table 3 indicate that the Kalman filter approach presented the lower RMSE for the overall experiment, presenting small variation throughout the phases. The reason why the Generalized momentum and the combined Kalman-momentum approach presented high RMSE values is because the time lag of each estimated torque, Note that the RMSE for the generalized momentum approach presented always higher RMSE than that of the combined Kalman-momentum approach, which is expected since the observed time lag in the former approach was greater than the observed in the latter.

The Kalman filter is the approach that offers better reliability in the estimation torque, thus this will be selected as the approach used for the ankle torque estimation described in the next chapter.

5 ANKLE TORQUE ESTIMATION

5.1 Experimental setup

Once the Kalman filter has been identified as the approach with best performance, it can be implemented to estimate the ankle torque for the case study described in section 3.4 (page 30). In Figure 25a is depicted the experimental setup for this case. As in section 4, the control system of the Anklebot is configured with a closed-loop control strategy that tracks the angular trajectory (Figure 25b), this time the ankle torque is considered the disturbance of the system. The control strategy was programmed to track a sinusoidal reference trajectory with amplitude and frequency equal to 0.174 radians (10 degrees) and 0.25 Hz respectively.

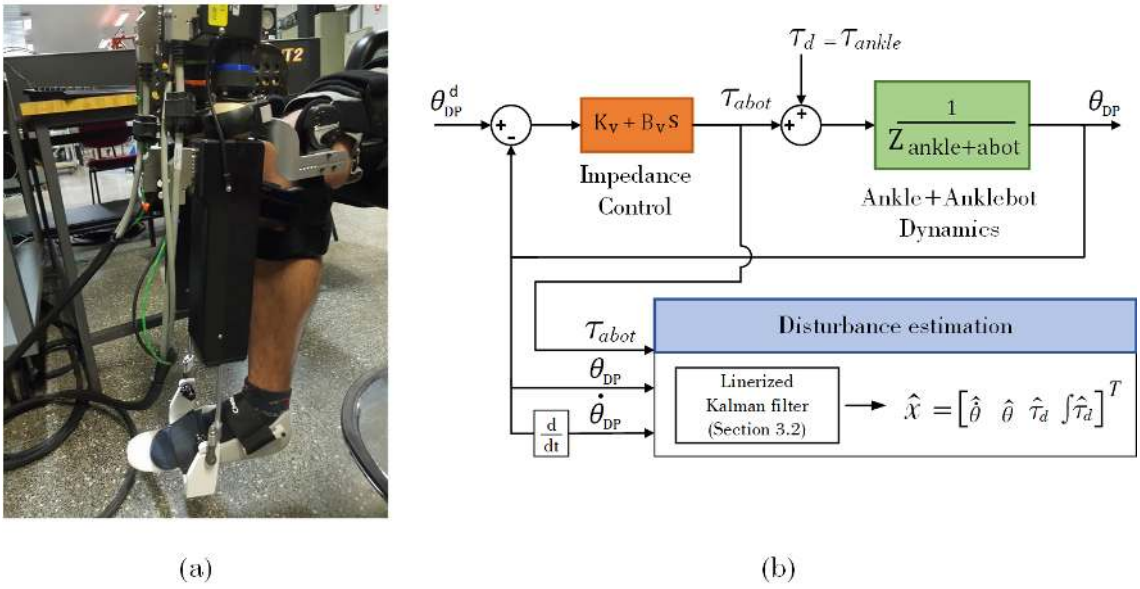

Figure 25: Configuration for ankle torque estimation.
(a) Experimental Setup (b) Control system strategy.

In lower limb robotic rehabilitation therapies, robots are capable of assisting the motion of patients in according with the configuration of its control strategy (**??**). In addition, during robotic therapies, subjects joint torques can be split into "passive" torques resulting from viscoelastic effects in the joint-surrounding tissue and "active" moments generated by muscles (RIENER et al., 2005). Based on this, here are defined four operation modes to represent the physical activity that the user may realize when interacting with the Anklebot: (1) passive mode, in which the user does not make any effort against the Anklebot movement; (2) active-1 mode in which the user makes efforts against the Anklebot movement by maintaining its ankle joint in a zero reference position; (3) active-2 mode in which the user makes efforts against the Anklebot by realizing the opposite movement of the robot and (4)

active-3 mode, in which the user makes efforts by cooperating with the Anklebot movement.

Four tests were performed in order to analyze the effect of varying the impedance control parameters and the human-robot physical interaction above described. Table 4 shows the configuration for each test.

Table 4: Configuration of tests for ankle torque estimation.

	IC parameters	Phase 1	Phase 2
Test 1	$K_v = 30$ N-m/rad	Duration (s): 12	Duration (s): 12
	$B_v = 5$ N-m-s/rad	Op. mode: passive	Op. mode: active-1
Test 2	$K_v = 60$ N-m/rad	Duration (s): 12	Duration (s): 12
	$B_v = 5$ N-m-s/rad	Op. mode: passive	Op. mode: active-1
Test 3	$K_v = 30$ N-m/rad	Duration (s): 12	Duration (s): 12
	$B_v = 5$ N-m-s/rad	Op. mode: passive	Op. mode: active-2
Test 4	$K_v = 0$ N-m/rad	Duration (s): 12	
	$B_v = 5$ N-m-s/rad	Op. mode: active-3	

5.2 Test 1: passive - active-1 operation mode and $K_v = 30$ N-m/rad

In the first phase of test 1, the subject ankle torque is asked first to perform the passive mode, by doing this, the subject will perform a passive ankle torque. After that, in phase 2 the subject is asked to perform the active-1 mode, thus, the subject will produce an ankle torque equals but opposite to that of the Anklebot, in such a way that the angle displacement will be zero.

Figure 26 show time responses for test 1. During first phase (0 to 12 seconds), the Anklebot led the ankle joint through the desired position, the reason that reference angular position is not reached, is because the programmed robot stiffness ($K_v = 30$ N-m/rad) is not enough higher than the ankle stiffness identified in section 3.4 ($K_{ankle} = 29.78$ N-m/rad). Furthermore, the estimated ankle torque (red line in Figure 26) exhibited a signal periodic with peak values around 1.2 N-m, this estimative can be understood as the passive ankle torque due to its viscoelastic muscle properties.

Whit respect to phase 2, since the K_v of the robot was not greater enough, the user was able to maintain the ankle joint in a zero reference position. The estimated ankle torque was expected to be opposite in amplitude of that of the Anklebot, as can be seen, $\hat{\tau}_{ankle}$ did not totally converge to the opposite amplitude of τ_{abot}. This can be evidenced if the the error between the root mean square value of estimated ankle torque and Anklebot

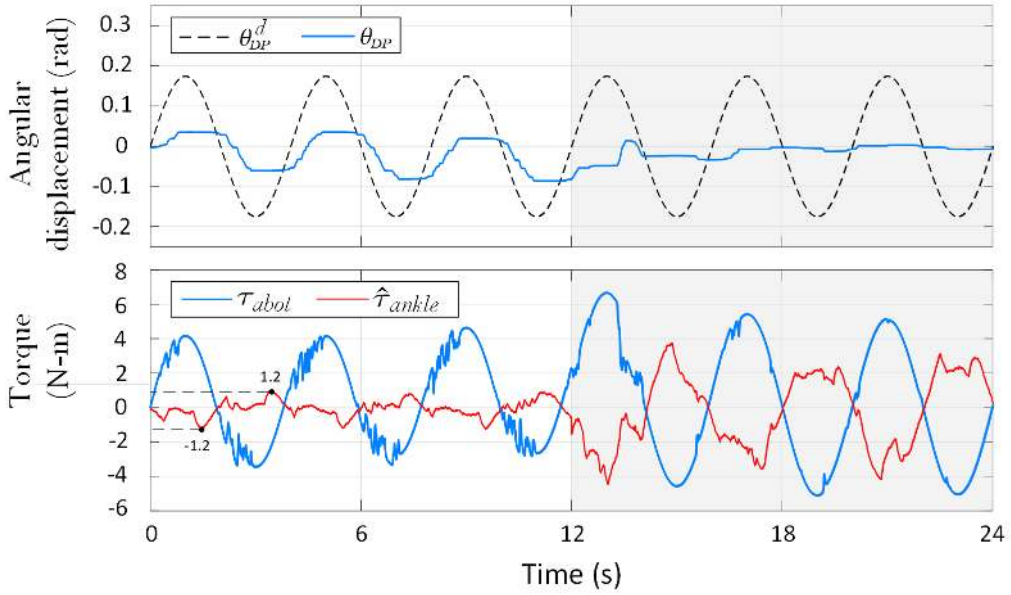

Figure 26: Ankle torque estimation for test 1. ☐ Phase 1 ■ Phase 2

torque is computed by using:

$$e = \mid RMS_{\hat{\tau}_d} - RMS_{\tau_{abot}} / RMS_{\tau_{abot}} \mid \cdot 100\% \tag{5.1}$$

thereby, during the active-1 operation mode, e, was 43.23 %.

5.3 Test 2: passive - active-1 operation mode and K_v = 60 N-m/rad

Unlike test 1, in test 2 the K_v parameter of impedance control was configured to 60 N-m/rad. By doing this, the subject will increase its ankle mechanical impedance (I_{ankle}, B_{ankle}, and K_{ankle} parameters) in order to make a greater physical effort in maintaining the ankle joint in a zero reference position. Figure 27 show the temporal responses for test 2.

In phase 1 The ankle torque estimation (red line), namely, the torque in passive mode operation, exhibited a signal periodic with peak values around 1.49 N-m, this estimate is in accordance with the founded in test 1. As it was expected, during phase 2 the user had more difficulty to maintain ankle joint position in zero reference, so the user dynamic exerted a greater ankle torque.

The error between the estimated ankle torque and Anklebot torque was computed by using Equation 5.1, thereby, during the active-1 operation mode, e, was 38.94 %. Compared with test 1, this error decreased, that is, the estimation improved when the virtual stiffness and ankle impedance became greater.

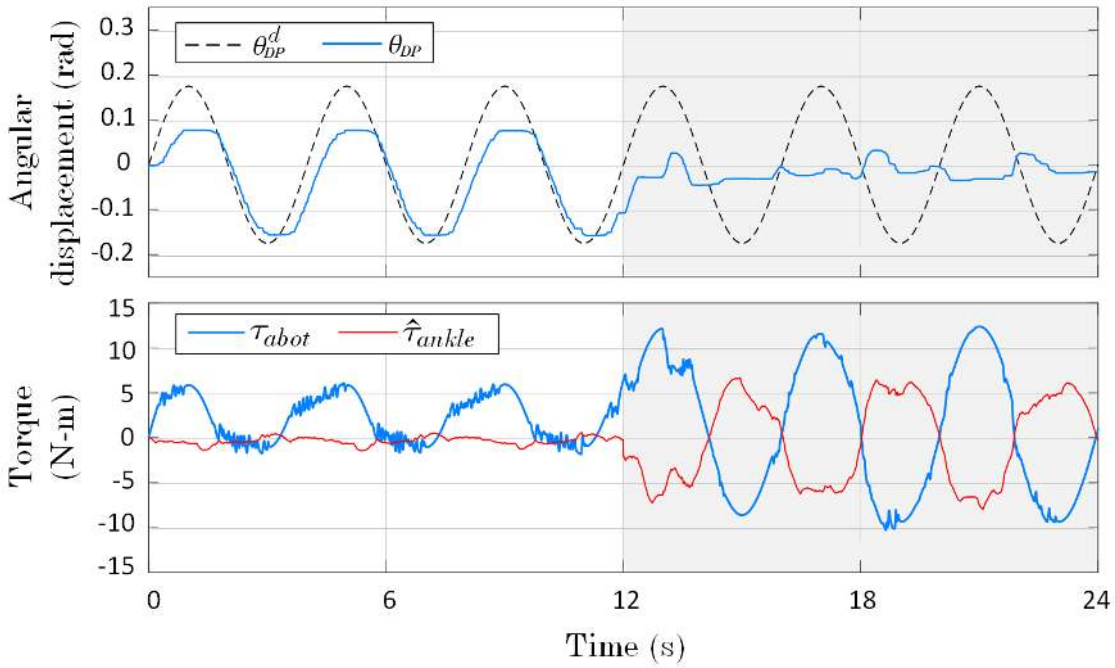

Figure 27: Ankle torque estimation for test 2.

5.4 Test 3: passive - active-2 operation mode and K_v = 30 N-m/rad

In test 3 the subject was asked to perform a passive mode in its phase 1, and to perform an active-2 operation mode for phase 2, The impedance control was configured with K_v = 30 N-m/rad so that, the user is able to do the opposite ankle joint movement of that imposed from the Anklebot. Figure 28 show the temporal responses for test 3.

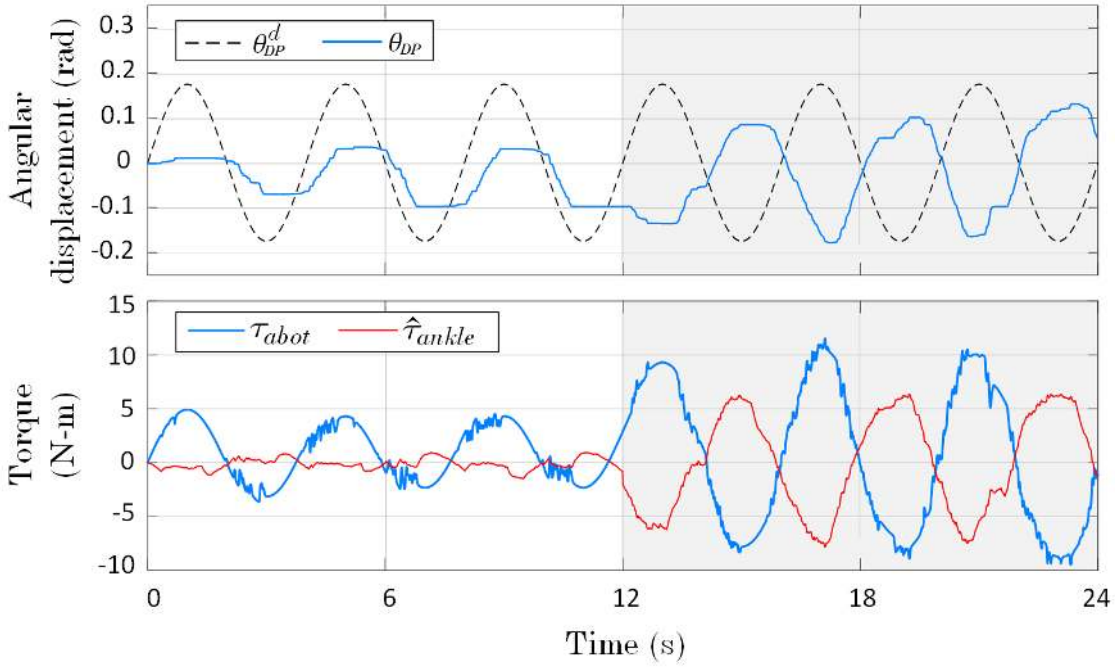

Figure 28: Ankle torque estimation for test 3.

The error between τ_{abot} and $\hat{\tau}_{ankle}$ was computed as 31.93 % by using Equation 5.1, namely, the estimated ankle torque was closer to the Anklebot torque for this test than the others, nevertheless, $\hat{\tau}_{ankle}$ was expected to be greater than τ_{abot}.

5.5 Test 4: passive - active-3 operation mode and K_v = 0 N-m/rad

In this test the Anklebot was configured to perform high backdriveability, so that the user can move its ankle to follow the desired angular trajectory with the least possible physical effort. The impedance control was configured with $K_v = 0$ N-m/rad and $B_v = 5$ N-m-s/rad, by doing this, the commanded Anklebot torque (Equation 3.5 on page 27) becomes $\tau_{abot} = \dot{\theta} B_v$. Figure 29 show the temporal responses for test 4.

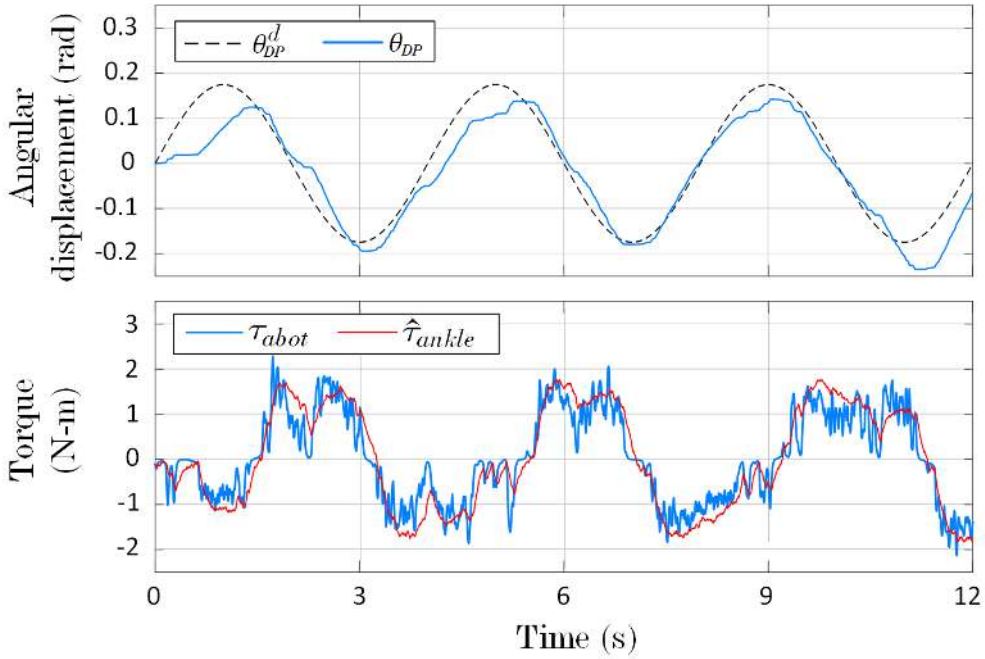

Figure 29: Ankle torque estimation for test 4.

Note that angular displacement is easily tracked and that the estimated ankle torque (red line) converges more closely to τ_{abot} than the other tests, this was expected since the user is transmitting the whole ankle torque to the Anklebot.

5.6 Conclusions of ankle torque estimation

In this chapter was presented the implementation results of the Kalman filter approach in the Anklebot robot to estimate the ankle torque of a voluntary subject. Four tests were performed considering the different types of strategies used in robotic therapies for lower limbs, in these tests, the impedance control of the Anklebot, commanded the actuator torque to move the ankle joint through a desired angular displacement, in the meantime,

the subject was asked to perform a set of defined operation modes.

The first three tests were split in two phases, where the subject performed passive operation mode during first phase and active operation mode during second phase.

In tests 1 and 2 the subject made efforts against the Anklebot movement to maintain its ankle joint in a zero reference position, they were programed each one with a different constant K_v parameter in its impedance control, to demonstrate the efficiency of the torque estimation despite changes in ankle+Anklebot dynamics. For the first phase of both tests, no matter which the K_v parameter was, the estimated passive ankle torques turned out to be close to each other. The validity of this estimates were verified by comparing the angle of such torques with a theoretical angle response of the ankle+Anklebot admittance function. With regard to phase 2, the estimated ankle torque of test 2 got closer to the Anklebot torque than that estimated in test 1, that is, the estimation improved when the K_v parameter and ankle impedance became greater.

The test 3 was implemented with the purpose to analyze the estimation approach when subject executes a greater ankle torque than the provided by the Anklebot. Although estimative was not as expected, it has to be taken into account that such estimative was compared with the commanded Anklebot torque instead of the physical actuator torque. In other words, since the subject is forcing the Anklebot to perform his ankle movement, the physical actuator torque is probably lower than that estimated for the ankle during phase 2. The backdriveability property of Anklebot implies that it generates an assistive torque precisely as desired, however, such torque is not available for a direct measurement. Another plausible explanation for the estimation results during phase 2 is that the ankle mechanical impedance parameters increased, so the model with which the torque was estimated experienced changes that affected its performance.

The fourth test was intended to evaluate the estimated ankle torque when the robot does not provide any assistance, as consequence, instead of help to reach the desired movement, the Anklebot receives the whole ankle torque from the subject. The estimation proved to be in accordance with what was previously stated, resulting in similar torques for the ankle and Anklebot.

6 CONCLUSIONS AND RECOMMENDATIONS

In this work an ankle torque estimation approach was developed on the Anklebot robot for lower limb rehabilitation. The approach was implemented on a voluntary subject wearing the Anklebot, the results proved to be successful for the passive torque and in most of the proposed modes of operation of active torque. This estimate can be an useful tool for robotic rehabilitation therapies, for example, isokinetic muscle strengthening training measures joint torques to analyze the functional recovery of stroke patients, such measurement is obtained through dynamometers, the torque estimation approach developed here could be an alternative solution to this measurement and also could be implemented in others robotic devices.

To achieve a proper estimation, it was required a detailed modeling of the ankle+Anklebot dynamics as well as the assumption of a disturbance model, in experiment results, the torque estimation performance was affected when subject modified his ankle mechanical impedance. Taking into account the above, the developed approach could be a good starting point to design a robust Kalman filter, that 1) avoids the identification of the ankle+Anklebot dynamics each time a new subject wears the Anklebot and 2) improve the performance estimation when ankle+Anklebot dynamics and controller's gains vary.

BIBLIOGRAPHY

ABHISHEK, G.; K., O. M. Disturbance-observer-based force estimation for haptic feedback. **Journal of Dynamic Systems, Measurement, and Control**, v. 133, n. 1, Dec 2010.

ANDREWS, J. Biomechanical measures of muscular effort. **Medicine and science in sports and exercise**, v. 15, n. 3, p. 199–207, 1983. ISSN 0195-9131.

BOHANNON, R. W. Manual muscle testing: does it meet the standards of an adequate screening test. **Clinical Rehabilitation**, v. 19, n. 6, p. 662–667, 2005. PMID: 16180603. Disponível em: <https://doi.org/10.1191/0269215505cr873oa>.

CAI, L. L. et al. Implications of assist-as-needed robotic step training after a complete spinal cord injury on intrinsic strategies of motor learning. **Journal of Neuroscience**, Society for Neuroscience, v. 26, n. 41, p. 10564–10568, 2006. ISSN 0270-6474.

DAMME, M. V. et al. Estimating robot and end-effector force from noisy actuator torque measurements. In: **IEEE International Conference on Robotics and Automation (ICRA)**. [S.l.: s.n.], 2011. p. 1108 – 1113.

EOM, K. S. et al. Disturbance observer based force control of robot manipulator without force sensor. In: **Robotics and Automation, 1998. Proceedings. 1998 IEEE International Conference on**. [S.l.: s.n.], 1998. v. 4, p. 3012–3017 vol.4. ISSN 1050-4729.

ERDEMIR, A. et al. Model-based estimation of muscle forces exerted during movements. **Clinical Biomechanics**, v. 22, n. 2, p. 131 – 154, Feb 2007. ISSN 0268-0033.

ESCOLAR, D. M. et al. Clinical evaluator reliability for quantitative and manual muscle testing measures of strength in children. **Muscle & Nerve**, v. 24, n. 6, p. 787–793. Disponível em: <https://onlinelibrary.wiley.com/doi/abs/10.1002/mus.1070>.

HUSSAIN, S.; XIE, S. Q.; JAMWAL, P. K. Adaptive impedance control of a robotic orthosis for gait rehabilitation. **IEEE Transactions on Cybernetics**, v. 43, n. 3, p. 1025–1034, June 2013. ISSN 2168-2267.

JUNG, J.; LEE, J.; HUH, K. Robust contact force estimation for robot manipulators in three-dimensional space. **Proceedings of the Institution of Mechanical Engineers, Part C: Journal of Mechanical Engineering Science**, SAGE Publications, v. 220, n. 9, p. 1317–1327, 2006.

KHAN, A. M. et al. Adaptive impedance control for upper limb assist exoskeleton. In: **2015 IEEE International Conference on Robotics and Automation (ICRA)**. [S.l.: s.n.], 2015. p. 4359–4366. ISSN 1050-4729.

KIM, J.; CHO, K.; CHOI, S. Lumped disturbance compensation using extended kalman filter for permanent magnet linear motor system. **International Journal of Control, Automation and Systems**, v. 14, n. 5, p. 1244–1253, Oct 2016. ISSN 2005-4092. Disponível em: <https://doi.org/10.1007/s12555-014-0400-1>.

KIM, W. et al. Development of a muscle circumference sensor to estimate torque of the human elbow joint. **Sensors and Actuators A: Physical**, v. 208, p. 95 – 103, 2014. ISSN 0924-4247.

KOMADA, S. et al. Development of a biofeedback therapeutic-exercise-supporting manipulator. **IEEE Transactions on Industrial Electronics**, v. 56, n. 10, p. 3914–3920, Oct 2009. ISSN 0278-0046.

LENZI, T. et al. Measuring human-robot interaction on wearable robots: A distributed approach. **Mechatronics**, v. 21, n. 6, p. 1123 – 1131, 2011. ISSN 0957-4158.

LLOYD, D. G.; BESIER, T. F. An emg-driven musculoskeletal model to estimate muscle forces and knee joint moments in vivo. **Journal of Biomechanics**, v. 36, n. 6, p. 765 – 776, Jun 2003. ISSN 0021-9290.

LUCA, A. D. et al. Collision detection and safe reaction with the dlr-iii lightweight manipulator arm. In: **Proceedings of the IEEE/RSJ International Conference on Intelligent Robots and Systems**. [S.l.: s.n.], 2006. p. 1623 –1630.

LUCA, A. D.; MATTONE, R. Actuator failure detection and isolation using generalized momenta. In: **Robotics and Automation, 2003. Proceedings. ICRA '03. IEEE International Conference on**. [S.l.: s.n.], 2003. v. 1, p. 634–639 vol.1. ISSN 1050-4729.

LUCA, A. D.; MATTONE, R. Actuator failure detection and isolation using generalized momenta. In: **Proceedings of the IEEE International Conference on Robotics and Automation**. [S.l.: s.n.], 2003. v. 1, p. 634–639.

LUCA, A. de; MATTONE, R. Sensorless robot collision detection and hybrid force-motion control. In: **Proceedings of the IEEE International Conference on Robotics and Automation**. [S.l.: s.n.], 2005. p. 999 – 1004.

LUNENBURGER, L.; COLOMBO, G.; RIENER, R. Biofeedback for robotic gait rehabilitation. **Journal of NeuroEngineering and Rehabilitation**, v. 4, n. 1, p. 1, 2007. ISSN 1743-0003.

MAQUIN, D. et al. 9th ifac symposium on fault detection, supervision and safety for technical processes safeprocess 2015 cartesian contact force estimation for robotic manipulators - a fault isolation perspective. **IFAC-PapersOnLine**, v. 48, n. 21, p. 1232 – 1237, 2015. ISSN 2405-8963.

MURAKAMI, T.; YU, F.; OHNISHI, K. Torque sensorless control in multidegree-of-freedom manipulator. **IEEE Transactions on Industrial Electronics**, v. 40, n. 2, p. 259–265, Apr 1993. ISSN 0278-0046.

MUSKE, K. R.; BADGWELL, T. A. Disturbance modeling for offset-free linear model predictive control. **Journal of Process Control**, v. 12, n. 5, p. 617–632, 2002. ISSN 0959-1524. Disponível em: <http://www.sciencedirect.com/science/article/pii/S0959152401000518>.

OHNISHI, K. A new servo method in mechatronics. In: **Transactions of Japanese Society of Electrical Engineers**. [S.l.: s.n.], 1987. v. 107 n.3, p. 83–86.

PARK, Y. J.; CHUNG, W. K. External torque-sensing algorithm for flexible-joint robot based on kalman filter. **Electronics Letters**, v. 49, n. 14, p. 877–878, July 2013. ISSN 0013-5194.

PEñA, G. G.; JAUREGUI, B.; SIQUEIRA, A. G. An optimized emg-driven model for patient torque estimation applied to rehabilitation robotics. In: **2015 12th Latin American Robotics Symposium and 2015 3rd Brazilian Symposium on Robotics (LARS-SBR)**. [S.l.: s.n.], 2015.

PRANGE, G. B. et al. Systematic review of the effect of robot-aided therapy on recovery of the hemiparetic arm after stroke. **Journal of rehabilitation research and development**, v. 43, n. 2, p. 171–184, 2006. ISSN 0748-7711.

PRIETO GUILLERMO, C.-d.-l.-C. R. L.-L. E. M. J. M. M. v. D. L. E. H. A. Emerging perspectives in stroke rehabilitation. In: _____. **Emerging Therapies in Neurorehabilitation**. Berlin, Heidelberg: Springer Berlin Heidelberg, 2014. p. 3–21. ISBN 978-3-642-38556-8.

RADKE, A.; GAO, Z. A survey of state and disturbance observers for practitioners. In: **2006 American Control Conference**. [S.l.: s.n.], 2006. p. 6 pp.–. ISSN 0743-1619.

RIENER, R. et al. Patient-cooperative strategies for robot-aided treadmill training: first experimental results. **IEEE Transactions on Neural Systems and Rehabilitation Engineering**, v. 13, n. 3, p. 380–394, Sept 2005. ISSN 1534-4320.

SICILIANO, B. et al. **Robotics: Modelling, Planning and Control**. London: Springer-Verlag, 2009.

STEFAN, L. S.; NATHAN, W. van de N.; HENK, N. H. Robust disturbance estimation for human robotic comanipulation. **International Journal of Robust and Nonlinear Control**, v. 24, n. 12, p. 1772?1796, Aug 1993. ISSN 1049-8923.

UGURLU, B. et al. A framework for sensorless torque estimation and control in wearable exoskeletons. In: **2012 12th IEEE International Workshop on Advanced Motion Control (AMC)**. [S.l.: s.n.], 2012. p. 1–7. ISSN 1943-6572.

_____. Proof of concept for robot-aided upper limb rehabilitation using disturbance observers. **IEEE Transactions on Human-Machine Systems**, v. 45, n. 1, p. 110–118, Feb 2015. ISSN 2168-2291.

WAHRBURG, A. et al. Cartesian contact force estimation for robotic manipulators using kalman filters and the generalized momentum. In: **2015 IEEE International Conference on Automation Science and Engineering (CASE)**. [S.l.: s.n.], 2015. p. 1230–1235. ISSN 2161-8070.

WELCH, G.; BISHOP, G. An introduction to the kalman filter: Siggraph 2001 course 8. In: **Computer Graphics, Annual Conference on Computer Graphics & Interactive Techniques**. [S.l.: s.n.], 2001. p. 12–17.